Article:
Voarintsoa, NRG, Matero, ISO, Railsback, LB et al. (10 more authors) (2019) Investigating the 8.2 ka event in northwestern Madagascar: Insight from data–model comparisons. Quaternary Science Reviews, 204. pp. 172-186. ISSN 0277-3791

https://doi.org/10.1016/j.quascirev.2018.11.030

Investigating the 8.2 ka event in northwestern Madagascar: insight from data–model comparisons

Ny Riavo G. Voarintsoa[1,*], Ilkka S.O. Matero[2], L. Bruce Railsback[1], Lauren Gregoire[2], Julia Tindall[2], Louise Sime[3], Hai Cheng[4,5], R. Lawrence Edwards[5], George A. Brook[6], Gayatri Kathayat[4], Xianglei Li[4], Amos Fety Michel Rakotondrazafy[7], and Marie Olga Madison Razanatseheno[7]

[1]*Department of Geology, University of Georgia, Athens, GA 30602-2501 U.S.A.*

[2]*University of Leeds, School of Earth and Environment, Leeds, LS2 9JT, UK*

[3]*Ice Dynamics and Paleoclimate, British Antarctic Survey, Cambridge CB3 0ET, UK*

[4]*Institute of Global Environmental Change, Xi'an Jiaotong University, Xi'an, Shaanxi 710049, P.R. China*

[5]*Department of Earth Sciences, University of Minnesota, Minneapolis, Minnesota 55455, U.S.A.*

[6]*Department of Geography, University of Georgia, Athens, Georgia, 30602-2502 U.S.A.*

[7]*Mention Sciences de la Terre et de l'Environnement, Domaine Sciences et Technologie, Université d'Antananarivo, Madagascar*

____

* Corresponding author:

E-mail address: nyriavony@gmail.com (Ny Riavo G. Voarintsoa)

Current address*: Institute of Earth Sciences, The Hebrew University in Jerusalem, Israel*

Abstract

The 8.2 ka event is a well-known cooling event in the Northern Hemisphere, but is poorly understood in Madagascar. Here, we compare paleoclimate data and outputs from paleoclimate simulations to better understand it. Records from Madagascar suggest two distinct sub-events (8.3 ka and 8.2 ka), that seem to correlate with records from northern high latitude. This could indicate causal relationships via changes in the Atlantic Meridional Overturning Circulation (AMOC) with changes in moisture source's $\delta^{18}O$, and changes in the mean position of the Inter-Tropical Convergence Zone (ITCZ), as climate modelling suggests. These two sub-events are also apparent in other terrestrial records, but the climatic signals are different. The prominent 8.2 ka sub-event records a clear antiphase relationship between the northern and southern hemisphere monsoons, whereas such relationship is less evident during the first 8.3 ka sub-event. Data–model comparison have also shown a mismatch between the paleoclimate data and the model outputs, the causes of which are more or less understood and may lie in the proxies, in the model, or in both data and model. Knowing that paleoclimate proxies and climate models produce different sets of variables, further research is needed to improve the data–model comparison approach, so that both paleoclimate data and paleoclimate models will better predict the likely climate status of a region during a specified time in the past with minimal uncertainties.

Keywords: Holocene; Speleothems; Stable isotopes; ITCZ–Monsoon; Madagascar; 8.2 ka event; Paleoclimate modeling; data–model comparisons; AMOC.

1. Introduction

The "8.2 ka event", an event that occurred between 8.5 and 7.9 thousand years (ka) ago (see Fig. 2 of Morrill et al., 2013a), is now well-defined as a clear abrupt climate perturbation of the early Holocene period (e.g. Alley et al., 1997; Barber et al., 1999; Morrill et al., 2013a). It was first identified in Switzerland (Zoller, 1960) and later in Canada (Hardy, 1977), but it was not scientifically recognized and named until the late 1990s, when more marine and terrestrial evidence was obtained (Alley et al. 1997). Overall, it was marked by regional cooling in the North Atlantic and surrounding regions (e.g., Johnsen et al., 1992; Alley et al., 1997; Marshall et al., 2007; Bond et al., 2001; Klitgaard-Kristensen et al., 1998; von Grafenstein et al., 1998; Barber et al., 1999; Alley and Ágústsdóttir, 2005), a 90% increase in forest fires in eastern Canada (e.g. Taylor et al., 1996; Alley et al. 1997), a decrease in atmospheric methane (Chappellaz et al., 1993; Blunier et al., 1995; Alley et al., 1997), a change in vegetation (e.g., Park et al., 2018), and significant climate anomalies in several regions such as changes to dry climate (Street-Perrott and Perrott, 1990; Gasse, 2000; Alley et al., 1997; Wang et al., 2005; Liu et al., 2013); changes in winter storm intensity (e.g., Oster et al., 2017), and changes in summer monsoon intensity (e.g. Cheng et al., 2009; Wang et al., 2005; Voarintsoa et al., 2017a).

Since the work of Alley and co-workers in 1997, the 8.2 ka event has attracted the attention of many scientists to investigate the causes (e.g. Alley and Ágústsdóttir, 2005; Barber et al., 1999; Bond et al., 2001; Clark et al., 2001; Clarke et al., 2004; Renssen et al., 2001; LeGrande et al., 2006; Vonmoos et al., 2006; Rohling and Pälike, 2005, Massé et al., 2008; Muller et al., 2009; Vare et al., 2009), the consequences (e.g. Thornalley et al., 2009; Andrews et al., 1999; Keigwin et al., 2005; Alley and Ágústsdóttir, 2005), the characteristics (e.g. Clark et al., 2001; Cheng et al., 2009; Retrum et al., 2013; Clarke et al., 2004; Hillaire-Marcel et al., 2007), and the climatic responses at different locations worldwide (e.g. Cheng et al., 2009; Boch et al., 2009; Alley and Ágústsdóttir, 2005; Rohling and Pälike, 2005; Morrill and Jacobsen, 2005; Park et al., 2018). Several climate simulations have been used to better understand the mechanisms behind and the main forcings of the 8.2 ka event (e.g. Goosse et al., 2002; Clarke et al., 2009; Renssen et al., 2001; Wiersma and Renssen, 2006; Tindall et al., 2009; Gordon et al., 2000; Pope et al., 2000; LeGrande et al., 2006; LeGrande and Schmidt, 2008; Bauer et al., 2004; Meissner and Clark, 2006; Tindall and Valdes, 2011; Renssen et al., 2001; Wiersma et al., 2006; Li et al., 2009; Bauer et al., 2004; Meissner and Clark 2006; LeGrande et al., 2006; LeGrande and Schmidt, 2008; Thomas et al. 2007; Tindall et al., 2009; Matero et al., 2017). Model outputs have been compared with empirical data (e.g. Renssen et al., 2001; Holmes et al., 2016; Wiersma and Renssen, 2006) to improve climate simulations and the simulated climate forcings known to have caused the 8.2 ka event. Given that there is a considerable body of information on the causes and magnitude of climate changes during the 8.2 ka event, data for this event could be thoroughly investigated to test the sensitivity of changes in ocean circulation in climate simulations. This would be a major step in improving climate prediction in future as noted elsewhere (e.g. Marshall et al., 2007; Wiersma et al., 2011; Morrill et al., 2013a), specifically in the Southern Hemisphere (SH).

Despite the extensive literature on the 8.2 ka event, it is also evident that more data are needed in the tropical regions of the SH (Morrill and Jacobsen, 2005; Morrill et al., 2013a; also see Fig. 4a of Wanner et al., 2011). Here we document in more detail the timing and structure of the 8.2 ka event in NW Madagascar, first reported by Voarintsoa et al. (2017c) in a study examining the last ca. 9800 years. We also examine links to global climate (oceanic and atmospheric) system, particularly ITCZ and monsoon behavior. To do this, we compare our stalagmite data with the output data from the climate simulation models of Matero et al., (2017), which is a new approach in the study of Madagascar's paleoclimate. We run additional analytical and statistical tests to better interpret the $\delta^{18}O$ and $\delta^{13}C$ values of the stalagmite and to understand the model outputs. For the analytical tests, we run Hendy tests on traceable spelean layers (~0.5 mm thick) to test for potential kinetic effects during $CaCO_3$ deposition. For the statistical tests, we used the Kolmorogorov-Smirnov (KS) two-sample test to determine if the distribution of precipitation between the control run and the 8.2 ka model scenarios is significantly different during interval studied. We also compared paleoclimate data from other locations than Madagascar with the model outputs to evaluate the model performance during the event period. Using both empirical and simulation data, we discuss how changes in AMOC during the 8.2 ka event may have impacted the climate of Madagascar, and the climate of other regions. We also discuss the differences between the model outputs and the paleoclimate data, and provide insights on the possible influence of the Aghulas Current, a warm current of South Atlantic, southwest off Madagascar (e.g., Beal et al., 2011; Rayner et al., 2011; Rühs et al., 2013) as recommendations to refine future climate models, when investigating changes in the AMOC.

FIG. 1 here (1.5–column fitting page)

2. Setting

Stalagmite ANJB-2 was collected from Anjohibe Cave (S15° 32' 33.3", E046° 53' 07.4"), in NW Madagascar (Fig. 1a). The environmental setting of the cave is described in Voarintsoa et al. (2017 b–c). The cave lies within the southern area of the Narinda Karst, which is the outcrop of a gently dipping (3–5° W) layer of Eocene limestone (Middleton and Middleton, 2002). Vegetation is dominated by savanna grasses with sparse endemic satra palms (Medemia nobilis) and other trees adapted to the long dry season and periodic fires (Brook et al., 1999; von Cabanis et al., 1969; Wright et al., 1996; also see Fig. 1b of Crowley and Samonds, 2013). NW Madagascar has a Tropical Savanna Climate (Aw; Köppen-Geiger climate classification), with a mean annual rainfall of ~1428 mm (historical data from 1901 to 2015; see Fig. 1b) and temperatures varying between 17°C and 36°C (1901–2015; see Fig. 1c). Summer rainfall is monsoonal (November-April), and it is linked to the seasonal migration of the ITCZ during austral summers (DGM, 2008; Jury, 2003; Tadross et al., 2008; Voarintsoa et al., 2017a, b). Temperatures inside the cave vary between 24.5°C and 26 °C, a range of temperature that approximates the external mean annual temperature in the region (Fig. 1c). When measurements were taken in May 2014, relative humidity in the cave varied between 72 and 87%, and PCO_2 varied between 400 and 500 ppm.

Table 1 here (landscape oriented)

FIG. 2 here (2–column fitting page)

3. Data and simulations

3.1. Paleoclimate data: Stalagmite ANJB-2

This study focuses on the radiometric dates, the stable oxygen and carbon isotope data, the changes in mineralogy, and other petrographic features of the basal 194 mm of Stalagmite ANJB-2, which includes the period of the 8.2 ka event. The $\delta^{18}O$ and $\delta^{13}C$ values reported herein were corrected to calcite if the spelean mineralogy was aragonite, to account for the latter's inherent fractionation of heavier isotopes (e.g. Tarutani et al., 1969; Rubinson and Clayton, 1969; Kim et al, 2007; Romanek et al., 1992). In addition to these stable isotope data, we took a new series of photomicrographs, using the Leica DMLP microscope that is equipped with Q-Capture. We combined these photomicrographs into a mosaic to illustrate the petrographic characteristics of the interval of interest (Fig. 2e). Our multiproxy investigation focused at the interval where the "8.2 ka event" is clearly defined and radiometrically constrained (Table 1; Fig. 2). This basal section of Stalagmite ANJB-2 is ideal for empirical data-simulation model comparison because it has a series of reliable and accurate U-Th dates (Table 1). Most of the twelve ^{230}Th ages obtained have uncertainties less than 50 years. Of the twelve dates, only one sample and its replicate (ANJB-2-120) were rejected because of the high detritus content, as indicated by low $^{230}Th/^{232}Th$ atomic ratios (ranging from 108 to 197e-06), the high porosity of the aragonite layer, easily identified on the hand sample, and because the age is not in stratigraphic order even when the large age uncertainties are considered (137 and 252 years for the duplicate samples). A StalAge model (Scholz and Hoffman, 2011) suggests an almost linear stalagmite growth rate of ca. 0.16 mm/yr, allowing us to obtain a sampling resolution of 3 to 8 years for the stable isotope records (n=370).

Common reliable paleoclimate proxies, including $\delta^{18}O$ and $\delta^{13}C$, mineralogy, and petrography (e.g. McDermott, 2004; Lachniet, 2009; Wong and Breecker, 2015; Railsback et al., 1994; Sletten et al., 2013; Asrat et al., 2007; Voarintsoa et al., 2017c; Fairchild and McMillan, 2007; see also Table 1 of Voarintsoa et al., 2017b), were used to provide a comprehensive understanding of the environmental changes during the 8.2 ka event in NW Madagascar. For a better interpretation of the stable oxygen and carbon isotope proxies, we investigated further the longitudinal correlation between $\delta^{18}O$ and $\delta^{13}C$ for the basal part of Stalagmite ANJB-2, using the parametric Pearson correlation coefficient. In this case, the mathematical form of the correlation was expressed using the Major Axis of the Model II Regression (Fig. 5). In addition to this correlation test, we collected three sets of four samples, consisting of ~50 to 100 µg powders of $CaCO_3$ extracted along three clearly visible and traceable layers with consistent thickness (~0.5 mm) at 1 mm (layer C), 207 mm (Layer B), and 218 mm (Layer A) from the top of the stalagmite to understand the degree of kinetic fractionation during the event period. For this layer-specific Hendy test, powder extraction was done using a handheld drill equipped with 0.2 mm-end drill cut. Samples were sent to the Alabama Stable Isotope Laboratory, and $\delta^{18}O$ and $\delta^{13}C$ measurements were done on a Delta V Plus at 50 °C. Layers A and B were examined to understand kinetic isotope effects (KIE) during the event period (respectively at the onset and near the end of the first 8.3 ka sub-event described later; Fig. 4), and Layer C was sampled as a modern analogue, i.e., to understand KIE under present conditions at the cave.

FIG. 3 here (1.5–column fitting page)

FIG. 4 here (2–column fitting page)

FIG. 5 here (1–column fitting page)

3.2. Paleoclimate simulations: Model description

The simulation of the 8.2 ka event that we used here is the published simulation of Matero et al. (2017), which uses the HadCM3 fully coupled atmosphere-ocean-vegetation GCM developed by the UK Met Office (Valdes et al., 2017; with the MOSES2.1 land-surface model and the TRIFFID dynamical vegetation model). The horizontal resolution of the atmosphere component of the model is 2.5° x 3.75°, with 19 unevenly spaced vertical levels. The ocean component has a horizontal resolution of 1.25° x 1.25°, a rigid lid, 20 unevenly spaced vertical levels, and maximum vertical resolution in the upper 300 m. Physical parameterizations in the ocean include thermodynamic sea-ice and eddy-mixing schemes. In this simulation, a 100–year long freshwater pulse with a peak value of 0.61 Sv was input into the Labrador Sea. The perturbation represented the meltwater from the collapse of an ice saddle over Hudson Bay entering the North Atlantic through the Hudson Strait (Carlson et al., 2008; Gregoire et al., 2012). In combination with background meltwater flux of 0.05 Sv input to the same area throughout the simulation, this meltwater flux is equivalent to a eustatic sea level rise of 4.2 meters over 400 years. The simulation produced a cooling pattern that is in good agreement with the amplitude and duration recorded in most of the robust European lake and North Atlantic sediment records (Morrill et al., 2013b), as well as the 160–year duration and 3°C amplitude of the 8.2 ka event recorded in ice cores from Greenland (Thomas et al., 2007; Kobashi et al., 2007).

FIG. 6 here (2–column fitting page)

3.3. Kolmogorov-Smirnov test on the model outputs

To better understand the significance of precipitation changes during the event period, we run the Kolmogorov-Smirnov (Massey, 1951 and references therein; Stephens, 1970) two-sample test between the control run and the 8.2 ka model scenarios, using the online KS-calculator of Kirkman (1996) and the free statistical software R. The Kolmorogorov-Smirnov test is a nonparametric test for overall equal distribution of two univariate samples, with the null hypothesis (H_0) being the two samples are taken from two random size populations (X and Y, with size m and n respectively) with equal distribution (i.e., $F_X(x) = F_Y(x)$ for all x, with F denoting the cumulative distribution function). The KS-test is a test of a goodness of fit, and it is based on the maximum absolute difference (D) between the empirical cumulative distribution functions (ECDF) of the two samples, expressed as $D_{m,n} = max\,(x)\,|S_{N1}(x) - S_{N2}(x)|$. Small D values indicate closeness of the two distributions, and large D values indicate the opposite.

FIG. 7 here (1–column fitting page)

3.4. Data-model comparison

Because paleoclimate proxies and climate models produce different sets of variables, we normalized and standardized both the simulated values from climate model and the paleoclimate proxy (Fig. 9). For normalization, we scaled the values to the [0,1] range using the minimum–maximum values scaling, using the following function: normalize <- function(x) {return ((x - min(x)) / (max(x) - min(x)))}. In this case, minimum values indicate less precipitation and maximum values more precipitation (Fig. 9a). For standardization, we calculated the mean and the standard deviation of every set of data. Then, we subtracted the mean from the value of each dataset, and divided the difference by the standard deviation using the following function: standardize <- function(x) {return (x – average (x)) / (stdev(x))}. These normalization and standardization approaches were done to ease comparison between models and proxy data and to ease interpretation of the results. Prior to calculating these values, we resampled the time series of each proxy data using the simple interpolation method of the AnalySeries 2.0 software (Paillard et al., 1996) so that the proxies share similar time series with the simulations.

4. Results

4.1. Proxies

For the period between 9.1 and 7.8 ka BP, we found a periodicity of ~800 years in the isotopic records and an overall trend towards higher delta values towards 7.8 ka BP (Fig. 4), which marks the end of the Malagasy Early Holocene Interval (Voarintsoa et al., 2017c). Within the interval of interest, we found two troughs (i.e., more negative isotopic values), separated by a short interval (~20 years) of higher $\delta^{18}O$ and $\delta^{13}C$. These two troughs will be referred in the discussion section as sub-events (to avoid potential confusion with the worldwide–named 8.2 ka event). Using the StalAge best fit age model of Stalagmite ANJB-2, the first sub-event (here named sub-event 8.3 ka) is defined between 8.37 and 8.25 ka BP, the second sub-event (here named sub-event 8.2 ka) between 8.23 and 8.10 ka BP, and each sub-event begins with an abrupt decrease in isotopic values from high to low values. The 8.3 ka sub-event has a trough of smaller amplitude (around –6.59‰ and –10.70‰ for $\delta^{18}O$ and $\delta^{13}C$, respectively), whereas the second sub-event, has a trough with greater amplitude (around –7.95‰ and –11.9‰ for $\delta^{18}O$ and $\delta^{13}C$, respectively), and it coincides in timing with the well-known "8.2 ka event" (e.g. Thomas et al., 2007; Vinther et al., 2009).

Microscopic observation of Stalagmite ANJB-2 thin sections allowed us to identify the following sequence of deposition. Type E surfaces are observed at the onset of both the 8.3 and 8.2 ka sub-events (Fig. 2), which closely coincide with the pulses identified in the isotopic records. Type E surfaces are layer-bounding surfaces where the previously deposited spelean layers were truncated/eroded by undersaturated dripwater during exceptionally wet conditions (see details in Railsback et al., 2013). In each case, the erosion is followed by the deposition of a laminated primary calcite layer. Each sub-event ends with the deposition of aragonite. The nature of the layer-bounding surface between calcite and aragonite is conformal, with no significant evidence of truncation of the previously deposited layer. A very simplified sketch portraying this stratigraphic succession is shown in Fig. S2.

We also found another trough, similar in amplitude with the 8.2 ka sub-event, around 8.7 ka BP (Fig. 3). Mineralogy in that interval is calcite, which overlies a Type E surface. The 8.7 ka event appears to be an abrupt event, and using the best fit chronology model from StalAge, it lasted only ~35 years. Although this 8.7 ka event may represent an important climatic event, we will mainly focus our discussion section around the globally recognized "8.2 ka event".

4.2. Simulations

Figure 6 depicts the time series of the simulated temperature and precipitation over NW Madagascar during the prominent 8.2 ka event in the '4.24m_100yr' –simulation in Matero et al., (2017). Overall, the climatic response in NW Madagascar to the 8.2 ka event forcing is not statistically significant. We did not find significant changes in temperature, such as has been noted by Morill et al. (2013b), and only a slight increase in the mean precipitation (up to 4%) was observed. However, large and abrupt increases in precipitation (~10%) were noticed over few short periods, mainly around model years 190, 230, 250, and 290 (i.e., around years 8251, 8210, 8190, and 8150). Such changes may be influenced by the southward shift in the mean position of the ITCZ in the southern tropics in response to the Labrador Sea freshwater forcing (Matero et al., 2017), and other climatic factors could additionally play some role (see Section 5.4.2).

FIG. 8 here (2–column fitting page)

FIG. 9 here (2–column fitting page)

4.3. Data-model comparison

Data-model comparison for NW Madagascar suggests that even though paleoclimate reconstructions from Stalagmite ANJB-2 and outputs from HadCM3 model simulation combine to indicate an overall wetter condition in Madagascar during the event period, a mismatch between proxies and simulation outputs exists. The speleothem proxy records show significant negative anomalies during the event period (Fig. 3; Section 4.1). In contrast, climate simulations show that changes are statistically non-significant (Fig. 6; Section 4.2). A KS-test between the control run and the 8.2 ka model scenarios shows that they have different distributions (D= 0.1165, p=0.028–

0.030, with a two-sided alternative hypothesis; Fig. 7). Kirkman online KS-test results also suggest that the control run is normally distributed (p=0.92), whereas the 8.2 ka simulation is not (p=0.09).

Figures 8 and 9 expand on this data-model comparison, in which paleoclimate data from Venezuela (Cariaco Basin), Brazil (Padre Cave), Spain (Kaite Cave), Oman (Qunf Cave), and China (Dongge Cave) are compared with the model output. Methods for comparison are discussed above (Section 3.4). Spatial and temporal distributions of the modelled precipitation anomalies is significantly different from one region to another (Figs. 8 and 9). In all regions, but China (Dongge Cave), KS-test suggest that the 8.2 ka model scenarios and the control run have different distribution (Fig. 9), with greatest D values (0.43) in Venezuela. Data–model comparisons also suggest a mismatch, the possible causes of which are discussed in Section 5.4.3.

5. Discussion

5.1. Speleothem stable isotopes and their implications

Variations in speleothem carbonate $\delta^{18}O$ and $\delta^{13}C$ are commonly used as proxies for paleoclimate and paleoenvironmental reconstruction (see review by Wong and Breecker, 2015; see also McDermott, 2004, and Lachniet, 2009). For a comprehensive review of karst systems and speleothem records, see Fairchild and Baker (2012). They can be influenced by conditions (1) inside the cave (e.g., temperature, ventilation, the magnitude of kinetic fractionation), (2) above and around the cave (e.g., geochemistry of the bedrock, nature and extent of vegetation cover), and (3) outside the cave that can be felt at short timescales (e.g. seasonality) and/or long timescales (e.g. glacial vs. interglacial period).

Inside caves, kinetic effects during carbonate precipitation influence isotopic composition of individual spelean layers, and can contribute to variability in speleothem records (e.g., Mickler et al., 2004, 2006; McDermott et al., 2006; Daëron et al., 2011). Kinetic effects may play a significant role in the isotopic fractionations accompanying degassing, evaporation, biologically mediated reactions, diffusion, and calcite precipitation along a spelean growth surface (Dietzel et al., 2009; DePaolo, 2011). In such scenarios, oxygen isotope fractionation between water and dissolved inorganic carbon (DIC) becomes fast, leading to high $\delta^{18}O$ values of precipitated carbonate that deviate from Hendy (1971)'s predicted thermodynamic equilibrium. Hendy (1971) suggested a theory that a progressive increase and the covariance between $\delta^{18}O$ and $\delta^{13}C$ in fast-growing calcite along a stalagmite growth axis indicate a deviation from equilibrium. This conclusion led to further investigation for covariations along selected speleothem laminae (i.e., the 'Hendy test'), which is a relatively difficult task to complete in most speleothems because individual lamina is too thin to sample. Because Delta Plus at 50°C allows a small sample size (50–100 μg of $CaCO_3$ powders), thus requiring only a very small trench (1.5 × 0.2 × 0.5 mm), performing a layer-specific Hendy test was possible on few selected layers (Section 3.1). Results of such exercises are shown in Figure 4, and they suggest that $\delta^{18}O$ and $\delta^{13}C$ are positively correlated. In addition, $\delta^{18}O$ and $\delta^{13}C$ of layer B (transition between sub-event 8.3 ka and sub-event 8.2 ka) and layer C (a layer equivalent to modern precipitates) become progressively enriched away from the stalagmite growth axis, likely suggesting a progressive evolution of the DIC during progressive CO_2 degassing and calcite precipitation (Mickler et al., 2006). In contrast, layer A (sampled at the onset of the 8.3 ka subevent) does not enrich away from the growth axis, suggesting that spelean layer may have been deposited in isotopic equilibrium with the cave drip water in a 100% relatively humid cave chamber (i.e., reflecting wet climate). A Major Axis Regression Hendy test along the growth axis of Stalagmite ANJB-2 also suggests that $\delta^{18}O$ and $\delta^{13}C$ are strongly correlated between 8.00 and 8.75 ka BP (r^2= 0.53), whereas before (9–8.75 ka

BP) and after (8–7.8 ka BP) this interval, a weaker correlation is observed (r^2= 0.31 and 0.16, respectively; Fig. 5). In summary, the modern cave temperature (~24.5–26 °C), the relative humidity (72–87%), the PCO_2 (~400–500 ppm), and the results from both layer-specific and along the growth axis Hendy tests suggest that kinetic fractionation occurs today, and it could also happen in the past in our study cave, except at the onset of the sub-event when relative humidity in the cave was predicted to be ~100%. Kinetic isotopic effects are a very common phenomenon in caves, where mean annual cave temperature exceeds 10°C (e.g., Baker et al., 2018).

Although kinetic effects may be one factor modifying the isotopic composition in stalagmite ANJB-2, it is additionally important to note that $\delta^{18}O$ values in tropical regions, like Madagascar, are influenced by the amount effect and seasonality (see Section 2.4 and Fig. 2 of Voarintsoa et al., 2017b; see also Dansgaard, 1964; Kurita et al., 2009; Lachniet, 2009; McDermott, 2004; and Rozanski et al., 1993), so our primary interpretation of speleothem $\delta^{18}O$ will be based on the amount effect. The replicability of $\delta^{13}C$ and $\delta^{18}O$ from previously published younger stalagmites (e.g., Burns et al., 2016; Voarintsoa et al., 2017b; Scroxton et al., 2017) from the same cave also suggests that stable isotope proxies from that cave can provide robust evidence that the isotope data can be interpreted directly in terms of external forcing factor. The 8.2 ka event is additionally replicated in a two-meter stalagmite from the same cave (currently in preparation by Wang and coworkers), in which the 8.2 ka event is marked by a major Type E, erosional, surface at which about 260 years (8.22 to 8.48 ka) of deposits were removed. While referring to Dorale and Liu (2009), who pointed out that changes in environmental conditions outside the cave can additionally lead to co-varying $\delta^{13}C$ and $\delta^{18}O$ along the growth axis of the speleothem, the correlation between $\delta^{13}C$ and $\delta^{18}O$ in Stalagmite ANJB-2 can best reflect a relationship between hydroclimate and vegetation during the event period. Hence, we interpret changes in $\delta^{13}C$ as proxy for climate–induced vegetation and hydrological changes during the event period.

5.2. Mineralogy and nature of layer-bounding surfaces: unconventional proxies for paleoenvironmental reconstruction

The stratigraphic succession of Type E surface, calcite, and aragonite for each event described in Section 4.1 can be explained as follows. The onset of each sub-event is marked by an exceptionally wet condition, as suggested by the presence of a Type E surface. Deposition of calcite indicates a continuation of the relatively wet conditions, which are also indicated by lower isotopic values. Primary calcite in speleothems generally indicates wet climate in a bi-mineralic stalagmite (e.g. Hill and Forti, 1997, p. 237–238; Railsback et al., 1994; Sletten et al., 2013; Voarintsoa et al., 2017a, b). Deposition of aragonite later in the event suggests that each event terminated with relatively drier conditions. Since aragonite has been interpreted to indicate warm and dry climates (Cabrol and Coudray, 1982; Moore 1956; Burton and Walter, 1987; Morse et al., 1997; Murray, 1954, Pobeguin, 1965, Thrailkill, 1971, Harmon et al., 1983), the presence of calcite layer above the Type E surface, i.e., after the onset of each event, could potentially suggest wetter conditions with subsequent evaporative cooling effect inside the cave (e.g. Cuthbert et al., 2014).

5.3. Paleoclimate reconstruction summary for NW Madagascar

The best fit StalAge model chronology (see Section 3.1, Fig. 2b), $\delta^{18}O$ and $\delta^{13}C$ values, mineralogy, and petrography of Stalagmite ANJB-2 combine to suggest a wetter climate in NW Madagascar at the onset of the 8.3 and the 8.2 ka sub-events. The 8.3 ka sub-event began with the formation of a Type E surface and low $\delta^{18}O$ and $\delta^{13}C$ values, followed by the deposition of calcite, all of which combine to indicate wet conditions. This first sub-event lasted approximately 110 years. The 8.2 ka sub-event also began with the formation of a Type E surface and low $\delta^{18}O$ and $\delta^{13}C$ values, followed by the deposition of calcite. It coincided with the most prominent event, widely known as the 8.2 ka event (Thomas et al., 2007; Vinther et al., 2009; Fig. 3), and it lasted ca. 140 years. The two events were separated by a short interval (ca. 20 years) of dry conditions, where a positive isotopic shift and aragonite were found in the record. This short dry period may record a weaker monsoon in Madagascar (Fig. 3), whereas the wet conditions may indicate a stronger monsoon.

FIG. 10 here (2–column fitting page)

5.4. Global comparison of paleoclimate data

5.4.1. Understanding linkages with low latitude records and monsoonal regions

Fig. 10B shows a time series comparison between speleothem $\delta^{18}O$ proxy data from Brazil, Oman, China, and Spain, along with a % Ti proxy from Venezuela. In that figure are presented the age uncertainties of the terrestrial records, except for the Cariaco Basin, where uncertainties were not specified in the publication source (Haug et al., 2001).

The two sub-events in Stalagmite ANJB-2 have also been identified in Stalagmite LV5 isotopic records from Kaite Cave in Spain (Domínguez-Villar et al., 2009; Fig. 10B.b), and in Stalagmite PAD07 isotopic records from Padre Cave in Brazil (Cheng et al., 2009), although the 8.3 ka sub-event is only marked by a small trough (Fig.10B.f). The LV5 records show similar timing for both sub-events, and the two troughs in the $\delta^{18}O$ time series during the event period were interpreted to be caused by the release of large amounts of fresh waters into the North Atlantic

(Domínguez-Villar et al., 2009). The PAD07 records show a double plunge structure (Cheng et al., 2009), indicating monsoon strengthening during the sub-event period. These PAD07 plunges also appear to coincide with the two cooling events in the subpolar North Atlantic (Clark et al., 2001; Ellison et al., 2006; Fig. 10A), potentially suggesting causal relationships (Cheng et al., 2009). This regional comparison may suggest that climate in Madagascar was in phase with climate in Brazil. Following the conclusion of Cheng et al. (2009), we could infer that monsoonal system in Madagascar (MM) was in phase with the South American Summer Monsoon (SASM), and that they may be influenced by changes in the North Atlantic region.

Comparison with other climatic records suggests a clear antiphase relationship between the northern and southern hemisphere monsoonal regions during the prominent 8.2 ka sub-event. This finding agrees with the conclusion of Cheng et al. (2009). This antiphase relationship could be inferred from the more positive $\delta^{18}O$ values in Stalagmite D4 (Cheng et al., 2009) and in Stalagmite Q5 (Fleitmann et al., 2003), and the low % Ti values in ODP 1002 (Haug et al., 2001), all suggesting drier conditions (i.e., weaker monsoon), *versus* the more negative $\delta^{18}O$ records from Stalagmite ANJB-2 and Stalagmite PAD07, suggesting wetter conditions (i.e., stronger monsoon). In contrast, the first 8.3 ka sub-event does not show a clear climate antiphase relationship between the two hemispheres, although a slight tendency towards wetter conditions may be inferred from the NH records. This climatic condition could be inferred from the more negative $\delta^{18}O$ values in Stalagmite D4 (Cheng et al., 2009), the more negative $\delta^{18}O$ in Stalagmite Q5 (Fleitmann et al., 2003), and the high % Ti in ODP 1002 (Haug et al., 2001) (Fig. 10B). Although such evidence is still open to further investigation, it could probably indicate not simply a southward shift but possibly a slight northward expansion of the ITCZ (see for example Frierson et al., 2007; Collins et al., 2011; Singarayer and Burrough, 2015).

5.4.2. Understanding linkages with high latitude records

In addition to the correlation previously observed between the stalagmite ANJB-2 $\delta^{18}O$ and $\delta^{13}C$ records and the Greenland ice core $\delta^{18}O$ records (Voarintsoa et al., 2017c), we also found another striking aspect. The two troughs seen in the records from Madagascar (Section 4.1; Fig. 3) appear to correlate with the two cooling events observed in the subpolar North Atlantic (Clark et al., 2001; Ellison et al., 2006), with an estimated time lag of 207 years and 167 years for the first and second sub-event, respectively (Fig. 10A). This estimated time lag considers the best fit chronology model of the speleothem records and the published chronology of Ellison et al. (2006), but they are also within the dating uncertainties of the records.

This correlation may suggest causal relationships, i.e., the inferred wet conditions and stronger monsoonal responses in NW Madagascar (Section 5.3) may have been related to southward displacements of the mean latitudinal position of the ITCZ (Matero et al., 2017), which in turn was influenced by the freshwater perturbations of the AMOC from the Laurentide Ice Sheet (e.g. Daley et al., 2011; Barber et al., 1999; Clark et al., 2001; Renssen et al., 2001; Clarke et al., 2004; LeGrande et al., 2006; Alley and Ágústsdóttir, 2005; Teller et al., 2002; Clarke et al., 2004). The perturbations can be summarized as follows, increased freshwater flux to the North Atlantic decreased the formation of the North Atlantic Deep Water, reducing the meridional heat transport (Barber et al., 1999; Clark et al., 2001; Daley et al., 2011; Vellinga and Wood 2002; Dong and Sutton 2002, 2007; Dahl et al. 2005; Zhang and Delworth 2005; Teller et al., 2002). This led to a significant change to the major downwelling limb of the AMOC (Ellison et al., 2006), resulting in widespread cooling in the NH regions (e.g. Clark et al., 2001; Thomas et al., 2007; see also fig. 8 of Morrill et al., 2013b) but warming in the SH regions (Wiersma et al., 2011; Wiersma and Renssen, 2006; Ljung et al., 2008). This climate response is similar to the “bipolar seesaw” effect, well-known during the last glacial (e.g. Crowley, 1992; Broecker, 1998), and this effect could have led to the southward displacement of the mean position of the ITCZ from a cooler NH (e.g., Chiang and Bitz, 2005; Broccoli et al., 2006) and/or an expansion of the African rain belt (e.g., Frierson et al., 2007; Collins et al., 2011; Singarayer and Burrough, 2015) during the prominent 8.2 ka abrupt event, responsible for an intensified monsoon in Madagascar.

The presence of the 8.3 ka and the 8.2 ka sub-events in several records (Fig.10B) could additionally suggest that the prominent "8.2 ka event", observed in several paleorecords and climate simulations as an anomaly event of the early Holocene, could have initially been an aftermath response to the first low-amplitude 8.3 ka sub-event. The trigger, the origin, and the mechanisms behind the 8.3 ka sub-event are still poorly known. However, three potential inter-dependent factors can be considered. First, the 8.3 ka sub-event could be explained by a linkage with the formation of the North Atlantic Deep Water, a main component of the AMOC. While analyzing deep-sea sediment core (MD99–2251) that was recovered from the southern limb of the Gardar Drift in the subpolar North Atlantic, Ellison et al. (2006) proposed a preconditioning of the North Atlantic by enhanced meltwater input, causing extensive cooling and freshening in the North Atlantic Ocean, further weakening the AMOC. This preconditioning hypothesis has been discussed in other studies (e.g. Hillaire-Marcel et al., 2007; Wiersma, 2008; Young et al., 2012; Matero et al., 2017). Second, it could be an influence and teleconnection with changes in the Southern Hemisphere, via the Aghulas Current (AC), a warm current adjacent to the southwestern coast of Madagascar and south of Africa. The AC carries a vast amount of heat southward from the warm and salty surface water of the tropical Indian Ocean to the cold Atlantic Ocean through the Mozambique Channel (e.g. Lutjeharms, 2006; Beal et al., 2011), often referred as the Aghulas water leakage (Rühs et al., 2013; De Ruijter et al., 1999). Although this leakage represents only a quarter of the return flow of the "global conveyor belt" (Broecker, 1991), it plays a role in global ocean heat fluxes between the ocean and the atmosphere (e.g. Fetter et al., 2007; Rühs et al., 2013), particularly in the global overturning circulation (e.g. Fetter et al., 2007; Lutjeharms, 2006; Rühs et al., 2013; Beal et al., 2011). The preconditioning of the North Atlantic discussed earlier could have not only enhanced extensive cooling and freshening in the North Atlantic Ocean but also enhanced warming in the South Atlantic, near the Aghulas Current. Such a temperature gradient could enhance heat transport to the NH via atmospheric and oceanic teleconnection, influencing melting of the Laurentide Ice Sheet, and could trigger the prominent freshwater outburst during the 8.2 ka event. A third factor could be associated with monsoons, but the mechanism may be more complicated as this must involve more complex land-ocean-atmosphere interactions.

5.4.3. Understanding the model-data mismatch

The data–model mismatch presented in Section 4.3 is not a new issue in data–model comparison studies (see for example Lunt et al., 2012; Phipps et al., 2013; Dee et al., 2015), and this problem could lie either in the climate model simulation, in the paleoclimate proxy, or in both model and data.

For the data, one possible explanation for the mismatch could be the current limited understanding of the controlling factors driving changes in the speleothem $\delta^{18}O$ and $\delta^{13}C$. Although the "amount effect" is believed to be the dominant factor influencing $\delta^{18}O$ in tropical regions, other internal and external factors could potentially complicate things (see Section 5.1). Kinetic isotopic effects inside the cave could be one factor accentuating the proxy signals (see Section 5.1). Limited accuracy in the paleoclimate chronology could also introduce uncertainty in paleoclimate reconstruction. One could also argue for potential changes in the moisture source for precipitation and in associated storm trajectories. The change in $\delta^{18}O$ values of the moisture source appears to be a reasonable explanation for these isotopic changes, assuming that the freshwater perturbations experienced within the AMOC had altered the moisture sources' $\delta^{18}O$ values and other associated climate variables. This could later be recorded in geological proxies such as the speleothem from Spain (e.g., Domínguez-Villar et al., 2009), and possibly the records from Madagascar (this study). Other climatic phenomena, such as the Indian Ocean Dipole (Saji et al., 1999; Zinke et al., 2004) and El-Nino Southern Oscillation (e.g. Brook et al., 1999) could also play additional roles in bringing occasional heavy rainfall to the target region, but the transfer time between climatic events to proxy records is not yet fully understood to provide comprehensive understanding of this.

For the model simulation, a possible explanation for the mismatch could lie in the model not properly reproducing the processes affecting changes in precipitation and temperature that may have driven the changes seen in the speleothem records. The model simulations may produce a year to year change. Another possible explanation could be linked to uncertainties associated with the output climatologies on a regional and temporal scale. Although GCM predictions of paleoclimate (Taylor et al., 2012) are quite consistent globally, there is still a considerable uncertainty in predicting regional precipitation fields and changes over time (e.g., Braconnot et al., 2012; Harrison et al., 2015). The model HadCM3 GCM used in this study (Matero et al., 2017) has been focused on simulating meltwater pulses produced by the Hudson Bay ice saddle collapse, using well-constrained meltwater scenarios as a function of melt rates that were inferred from known processes of ice retreat (Gregoire et al., 2012) and as a function of melt volumes derived from sea level records (Törnqvist and Hijma, 2012; Lambeck et al., 2014). The forcing in the study principally shows the shift in the ITCZ; however, the expected changes could be more complex than that. In addition, quantitative constraints on the modeled amount of precipitation are still limited, and it is also possible to assume that the forcing was not only responsible for the latitudinal shift but also it could have caused an expansion/contraction of the tropical rain belt (e.g., Singarayer and Burrough, 2015). It is also very likely that "a model may represent the observed change in one region and fail to capture the correct change in another" (Braconnot et al., 2012). Hence, future model-data comparison could consider developing a modelling study focusing on simulating warming of the Aghulas Current, and its linkage to the AMOC during the same event period, as this could possibly bring a better understanding on the climate linkage between cold deep waters and warm surface currents, and a better understanding of the relationship between the northern latitudes, the tropics, and the monsoonal regions.

Finally, one cannot ignore that a major limitation in data–model comparison still lies in the different sets of variables produced by paleoclimate proxies and climate models. On one hand, models directly simulate physical variables such as temperature or precipitation, whereas paleoclimate proxies, on the other hand, are preserved physical characteristics of the past presumed to record climatic changes over time, and their interpretation to reflect climate is based on the physical and chemical processes associated with their formation. Obviously, a lot of efforts from both paleoclimate modelers and paleoclimate scientists are still needed to improve this data–model comparison approach to better predict paleoclimate.

6. Conclusions

This data-model comparison study has led to the following conclusions. First, stalagmite records from Madagascar suggest two intervals of wet conditions during sub-events 8.3 ka and 8.2 ka, separated by ca. 20 years of drier conditions. The two wet phases appear to be linked to two cooling events in the subpolar North Atlantic via oceanic and atmospheric teleconnections. Although there are still uncertainties regarding temporal evolution of the meltwater flux to the

North Atlantic from the melting Laurentide Ice Sheet, and although our simulations (Matero et al., 2017) do not have a two-stage sequence of freshwater forcing, the two distinct cooling events in the subpolar North Atlantic (Fig. 5A; Clark et al., 2001; Ellison et al., 2006) seem to have left signatures in the records from NW Madagascar (e.g., changes in moisture source's $\delta^{18}O$). Model HadCM3 outputs suggest that the period of increased precipitation and monsoon intensification in NW Madagascar was consistent with the southward shift of the mean position of the ITCZ, which was linked to the weakening of the AMOC after the abrupt influx of freshwater into the North Atlantic (Barber et al., 1999; Clarke et al., 2001; Daley et al., 2011; Vellinga and Wood 2002; Dong and Sutton 2002, 2007; Dahl et al. 2005; Zhang and Delworth 2005; Matero et al., 2017). The global significance of the records from Madagascar confirms the need for more high-resolution paleoclimate data from the Southern Hemisphere, particularly within the tropics. The data are needed to improve the data–model comparisons.

Inter-comparison of paleoclimate time series suggests a clearer antiphase relationship between the Southern and Northern Hemisphere monsoonal regions during the second 8.2 ka sub-event compared to the first 8.3 ka sub-event. This demonstrates the complexity of land-atmosphere-ocean interactions. Data-model comparisons further suggest a mismatch between the simulated climate anomalies and the paleoclimate time series, the causes of which are more or less understood, but much effort from climate modelers and paleoclimate scientists is still needed to improve such comparison, so that both paleoclimate data and paleoclimate model will predict the likely climate status of a region during a specified time in the past with minimum uncertainties.

Acknowledgment

This research was supported by the following grants: (1) the National Natural Science Foundation of China (NSFC 41230524 and 41561144003) to Hai Cheng, (2) the NERC grant NE/L002574/1 to Ilkka S.O. Matero, (3) the Geological Society of America Research Grant (GSA 11166-16) and John Montagne Fund Award to N. Voarintsoa, (4) the Miriam Watts-Wheeler Graduate Student Grant from the Department of Geology at UGA to N. Voarintsoa, and (5) the International Association of Sedimentology Post-Graduate Grant to N. Voarintsoa. We also thank the Schlumberger Foundation for providing additional support to N. Voarintsoa's research. We thank the Department of Geology at the University of Antananarivo, in Madagascar, the Ministry of Energy and Mines, the local village and guides in Majunga for facilitating our research in Madagascar. We specifically thank the former Department Head of the Department of Geology at the University of Antananarivo, for giving permission to do field expedition in Madagascar. We thank Prof. Paul Schroeder for giving us access to use the X-ray diffractometer of the Geology Department to conduct analysis on the mineralogy of Stalagmite ANJB-2. We thank Dr. Lixin Wang and Dr. Liz Keller for many productive discussions of the 8.2 ka event, and Dr. Joe Lambert for his prompt service analyzing our samples for stable isotopes. We thank Dr. Domínguez-Villar for sharing his Kaite Cave data with us. Finally, we thank Prof. Andy Baker for sharing unpublished $\delta^{18}O$ metadata analyses of drip water, allowing us to better understand factors controlling $\delta^{18}O$ in caves.

References

Alley, R.B., Ágústsdóttir, A.M., 2005. The 8k event: cause and consequences of a major Holocene abrupt climate change. Quaternary Sci Rev 24, 1123–1149.

Alley, R.B., Mayewski, P.A., Sowers, T., Stuiver, M., Taylor, K.C., Clark, P.U., 1997. Holocene climatic instability: A prominent, widespread event 8200 yr ago. Geology 25, 483–486.

Andrews, J.T., Keigwin, L., Hall, F., Jennings, A.E., 1999. Abrupt deglaciation events and Holocene palaeoceanography from high-resolution cores, Cartwright Saddle, Labrador Shelf, Canada. J Quaternary Sci 14, 383–397.

Asrat, A., Baker, A., Mohammed, M.U., Leng, M.J., Van Calsteren, P., Smith, C., 2007. A high-resolution multi-proxy stalagmite record from Mechara, Southeastern Ethiopia: palaeohydrological implications for speleothem palaeoclimate reconstruction. J Quaternary Sci 22, 53–63.

Baker, A., Duan, W., Cuthbert, M., Treble, P., Banner, J., & Hankin, S. (2018, March 8). Climatic influences on the offset between d18O of cave drip waters and precipitation inferred from global monitoring data. https://doi.org/10.31223/osf.io/h4pr6

Barber, D.C., Dyke, A., Hillaire-Marcel, C., Jennings, A.E., Andrews, J.T., Kerwin, M.W., Bilodeau, G., McNeely, R., Southon, J., Morehead, M.D., Gagnon, J.M., 1999. Forcing of the cold event of 8,200 years ago by catastrophic drainage of Laurentide lakes. Nature 400, 344–348.

Bauer, E., Ganopolski, A., Montoya, M., 2004. Simulation of the cold climate event 8200 years ago by meltwater out-burst from lake Agassiz. Paleoceanography 19, PA3014. http://dx.doi.org/10.1029/2004PA001030.

Beal, L.M., De Ruijter, W.P.M., Biastoch, A., Zahn, R., 136, S.W.I.W.G., 2011. On the role of the Agulhas system in ocean circulation and climate. Nature 472, 429-436.

Blunier, T., Chappellaz, J., Schwander, J., Stauffer, B., and Raynaud, D., 1995. Variations in atmospheric methane concentration during the Holocene Epoch: Nature 374, 46–49.

Boch, R., C Spötl, and J. Kramers. 2009, High-resolution isotope records of early Holocene rapid climate change from two coeval stalagmites of Katerloch Cave, Austria. Quaternary Science Reviews, Vol. 28, pp. 2527-2538. doi:10.1016/j.quascirev.2009.05.015

Bond, G., Kromer, B., Beer, J., Muscheler, R., Evans, M.N., Showers, W., Hoffmann, S., Lotti-Bond, R., Hajdas, I., Bonani, G., 2001. Persistent solar influence on north Atlantic climate during the Holocene. Science 294, 2130-2136.

Braconnot, P., Harrison, S.P., Kageyama, M., Bartlein, P.J., Masson-Delmotte, V., Abe-Ouchi, A., Otto-Bliesner, B., Zhao, Y., 2012. Evaluation of climate models using palaeoclimatic data. Nat Clim Change 2, 417.

Broccoli, A.J., Dahl, K.A., Stouffer, R.J., 2006. Response of the ITCZ to Northern Hemisphere cooling. Geophys Res Lett 33.

Broecker, W.S., 1991. The Great Ocean Conveyor. Oceanography 4, 79-89.

Broecker, W.S., 1992. The Great Ocean Conveyor. Global Warming : Physics and Facts 247, 129–161.

Broecker, W.S., 1998. Paleocean circulation during the last deglaciation: A bipolar seesaw? Paleoceanography 13, 119–121

Brook, G.A., Rafter, M.A., Railsback, L.B., Sheen, S.W., Lundberg, J., 1999. A high-resolution proxy record of rainfall and ENSO since AD 1550 from layering in stalagmites from Anjohibe Cave, Madagascar. Holocene 9, 695–705.

Burton, E.A., Walter, L.M., 1987. Relative precipitation rates of aragonite and Mg calcite from seawater: Temperature or carbonate ion control? Geology 15, 111–114

Cabrol, P., Coudray, J., 1982. Climatic fluctuations influence the genesis and diagenesis of carbonate speleothems in southwestern France. Natl. Spel. Soc. Bul. 44, 112–117.

Carlson, A.E., LeGrande, A.N., Oppo, D.W., Came, R.E., Schmidt, G.A., Anslow, F.S., Licciardi, J.M., Obbink, E.A., 2008. Rapid early Holocene deglaciation of the Laurentide ice sheet. Nat. Geosci. 1, 620–624.

Chappellaz, J., Blunier, T., Raynaud, D., Barnola, J. M., Schwander, J., and Stauffer, B., 1993. Synchronous changes in atmospheric CH_4 and Greenland climate between 40 and 8 kyr BP. Nature 366, 443–445.

Chen, T.-C., 2003. Maintenance of Summer Monsoon Circulations: A Planetary-Scale Perspective. J Climate 16, 2022-2037.

Cheng, H., Edwards, R.L., Shen, C.C., Polyak, V.J., Asmerom, Y., Woodhead, J., Hellstrom, J., Wang, Y.J., Kong, X.G., Spotl, C., Wang, X.F., Alexander, E.C., 2013. Improvements in Th-230 dating, Th-230 and U-234 half-life values, and U-Th isotopic measurements by multi-collector inductively coupled plasma mass spectrometry. Earth Planet Sc Lett 371, 82-91.

Cheng, H., Fleitmann, D., Edwards, R.L., Wang, X.F., Cruz, F.W., Auler, A.S., Mangini, A., Wang, Y.J., Kong, X.G., Burns, S.J., Matter, A., 2009. Timing and structure of the 8.2 kyr BP event inferred from delta O-18 records of stalagmites from China, Oman, and Brazil. Geology 37, 1007–1010.

Chiang, J.C.H., Bitz, C.M., 2005. Influence of high latitude ice cover on the marine Intertropical Convergence Zone. Clim Dynam 25, 477–496.

Clark, P. U., Marshall, S. J., Clarke, G. K. C., Hostetler, S. W., Licciardi, J. M., Teller, J. T., 2001. Freshwater Forcing of Abrupt Climate Change During the Last Glaciation. Science 293, 283–287.

Clarke, G.K.C., Leverington, D.W., Teller, J.T., Dyke, A.S., 2004. Paleohydraulics of the last outburst flood from glacial lake Agassiz and the 8200 BP cold event. Quat. Sci. Rev. 23, 389–407.

Clarke, G.K.C., Bush, A.B.G., Bush, J.W.M., 2009. Freshwater discharge, sediment transport, and modeled climate impacts of the final drainage of glacial Lake Agassiz. J Climate 22, 2161–2180.

Collins, J.A., Schefuß, E., Heslop, D., Mulitza, S., Prange, M., Zabel, M., Tjallingii, R., Dokken, T.M., Huang, E., Mackensen, A., Schulz, M., Tian, J., Zarriess, M., Wefer, G., 2010. Interhemispheric symmetry of the tropical African rainbelt over the past 23,000 years. Nat Geosci 4, 42.

Crowley, T. J., 1992, North Atlantic Deep Water cools the Southern Hemisphere: Paleoceanography 7, 489–497.

Crowley, B.E., Samonds, K.E., 2013. Stable carbon isotope values confirm a recent increase in grasslands in northwestern Madagascar. Holocene 23, 1066–1073.

Cuthbert, M.O., Rau, G.C., Andersen, M.S., Roshan, H., Rutlidge, H., Marjo, C.E., Markowska, M., Jex, C.N., Graham, P.W., Mariethoz, G., Acworth, R.I., Baker, A., 2014. Evaporative cooling of speleothem drip water. Sci Rep-Uk 4, 5162.

Daëron, M., Guo, W., Eiler, J., Genty, D., Blamart, D., Boch, R., Drysdale, R., Maire, R., Wainer, K., Zanchetta, G., 2011. 13C18O clumping in speleothems: Observations from natural caves and precipitation experiments. Geochim Cosmochim Ac 75, 3303-3317.

Dahl, K., Broccoli, A., Stouffer, R., 2005. Assessing the role of North Atlantic freshwater forcing in millennial scale climate variability: a tropical Atlantic perspective. Clim Dynam 24, 325–346, 10.1007/s00382-004-0499-5.

Daley, T.J., Thomas, E.R., Holmes, J.A., Street-Perrott, F.A., Chapman, M.R., Tindall, J.C., Valdes, P.J., Loader, N.J., Marshall, J.D., Wolff, E.W., Hopley, P.J., Atkinson, T., Barber, K.E., Fisher, E.H., Robertson, I., Hughes, P.D.M., Roberts, C.N., 2011. The 8200 yr BP cold event in stable isotope records from the north Atlantic region. Glob. Planet. Change 79, 288–302.

Dansgaard, W., 1964. Stable isotopes in precipitation. Tellus 16, 436–468.

Dee, S., Emile-Geay, J., Evans, M.N., Allam, A., Steig, E.J., Thompson, D.M., 2015. PRYSM: An open-source framework for PRoxY System Modeling, with applications to oxygen-isotope systems. Journal of Advances in Modeling Earth Systems 7, 1220-1247.

Delworth, T. L., Clark, P. U., Holland, M., Johns, W. E., Kuhlbrodt, T., Lynch-Stieglitz, J., Morrill, C., Seager, R., Weaver, A. J., Zhang, R., 2008. The potential for abrupt change in the Atlantic Meridional Overturning Circulation, in: Abrupt Climate Change. A report by the U.S. Climate Change Science Program and the Subcommittee on Global Change Research. U.S. Geological Survey Reston, VA, 117–162.

DePaolo, D.J., 2011. Surface kinetic model for isotopic and trace element fraction- ation during precipitation of calcite from aqueous solutions. Geochim. Cosmochim. Acta 75, 1039–1056. http://dx.doi.org/10.1016/j.gca.2010.11.020.

DGM [Direction Générale de la Météorologie], 2008. Le changement climatique à Madagascar.

Dietzel, M., Tang, J.W., Leis, A., Kohler, S.J., 2009. Oxygen isotopic fractionation during inorganic calcite precipitation–effects of temperature, precipitation rate and pH. Chemical Geology 268, 107–115.

Dong, B.W., Sutton, R.T., 2002. Adjustment of the coupled ocean-atmosphere system to a sudden change in the Thermohaline Circulation. Geophys Res Lett 29.

Dong, B., and Sutton, R.T., 2007 Enhancement of ENSO variability by a weakened Atlantic thermohaline circulation in a coupled GCM. J Climate 20, 4920–4939.

Dorale, J.A., Liu, Z., 2009. Limitations of Hendy Test criteria in judging the paleoclimatic suitability of speleothems and the need for replication. J. Cave Karst Stud. 71, 73–80.

Ellison, C.R.W., Chapman, M.R., Hall, I.R., 2006. Surface and deep ocean interactions during the cold climate event 8200 years ago. Science 312, 1929–1932, doi: 10.1126/science.1127213.

Fairchild, I.J., Baker, A., 2012. Speleothem Science: From Processes to Past Environments. Wiley-Blackwell.

Fairchild, I.J., McMillan, E.A., 2007. Speleothems as indicators of wet and dry periods. Intl J Speleol 36, 69–74.

Fetter, A., Lutjeharms, J.R.E., Matano, R.P., 2007. Atmospheric driving forces for the Agulhas Current in the subtropics. Geophys Res Lett 34.

Fleitmann, D., Burns, S.J., Mudelsee, M., Neff, U., Kramers, J., Mangini, A., Matter, A., 2003. Holocene forcing of the Indian monsoon recorded in a stalagmite from Southern Oman. Science 300, 1737-1739.

Frierson, D.M.W., Lu, J., Chen, G., 2007. Width of the Hadley cell in simple and comprehensive general circulation models. Geophys Res Lett 34.

Gasse, F., 2000. Hydrological changes in the African tropics since the last Glacial maximum. Quat. Sci. Rev. 19, 189–211.

Goosse, H., Renssen, H., Selten, F.M., Haarsma, R.J., Opsteegh, J.D., 2002. Potential causes of abrupt climate events: A numerical study with a three-dimensional climate model. Geophys. Res. Lett. 29, doi:10.1029/2002GL014993.

Gordon, A.L., 1986. Interocean exchange of thermocline water. J Geophys Res 91, 5037–5046.

Gordon, C., Cooper, C., Senior, C.A., Banks, H., Gregory, J.M., Johns, T.C., Mitchell, J.F.B., Wood, R.A., 2000. The simulation of SST, sea ice extents and ocean heat transports in a version of the Hadley Centre coupled model without flux adjustments. Climate Dynamics 16, 147–168.

Gregoire, L.J., Payne, A.J., Valdes, P.J., 2012. Deglacial rapid sea level rises caused by ice-sheet saddle collapses. Nature 487, 219–222.

Hardy, L., 1977. La déglaciation et les épisodes lacustre et marin sur les versants de la partie québécoise des basses terres de la baie de James. Geogr. Phys. Quat. 31, 261–273.

Harmon, R.S., Atkinson, T.C., Atkinson, J.L., 1983. The mineralogy of Castleguard Cave, Columbia Icefields, Alberta Canada. Arctic and Alpine Research 15, 503–516.

Harrison, S.P., Bartlein, P.J., Izumi, K., Li, G., Annan, J., Hargreaves, J., Braconnot, P., Kageyama, M., 2015. Evaluation of CMIP5 palaeo-simulations to improve climate projections. Nat Clim Change 5, 735.

Haug, G.H., Hughen, K.A., Sigman, D.M., Peterson, L.C., Rohl, U., 2001. Southward migration of the intertropical convergence zone through the Holocene. Science 293, 1304–1308.

Hendy, C.H., 1971. The isotopic geochemistry of speleothems. I: The calculation of the effects of different modes of formation on the isotopic composition of speleothems and their applicability as palaeoclimatic indicators. Geochim. Cosmochim. Acta 35, 801–824.

Hill, C., Forti, P., 1997. Cave Minerals of the World. National Speleological Society, Huntsville, AL (463 p).

Hillaire-Marcel, C., de Vernal, A., Piper, D.J.W., 2007. Lake Agassiz final drainage event in the northwest north Atlantic. Geophys. Res. Lett. 34, L15601. http://dx.doi.org/10.1029/2007GL030396.

Holmes, J.A., Tindall, J., Roberts, N., Marshall, W., Marshall, J.D., Bingham, A., Feeser, I., O'Connell, M., Atkinson, T., Jourdan, A.-L., March, A., Fisher, E.H., 2016. Lake isotope records of the 8200-year cooling event in western Ireland: Comparison with model simulations. Quaternary Sci Rev 131, Part B, 341-349.

Jaffey, A.H., Flynn, K.F., Glendenin, L.E., Bentley, W.C., Essling, A.M., 1971. Precision measurement of half-lives and specific activities of 235U and 238U. Phys. Rev. 4, 1889–1906.

Johnsen, S.J., Clausen, H.B., Dansgaard, W., Fuhrer, K., Gundestrup, N., Hammer, C.U., Iversen, P., Jouzel, J., Stauffer, B., Steffensen, J.P., 1992. Irregular glacial interstadials recorded in a new Greenland ice core. Nature 359, 311–313.

Jury, M.R., 2003. The Climate of Madagascar, in: Goodman, S.M., Benstead, J.P. (Eds.), The Natural History of Madagascar, Chicago: University of Chicago, pp. 75–87.

Keigwin, L.D., Sachs, J.P., Rosenthal, Y., Boyle, E.A., 2005. The 8200 year BP event in the slope water system, western subpolar North Atlantic. Paleoceanography 20, PA2003. doi:10.1029/2004PA001074.

Kim, S.T., O'Neil, J.R., Hillaire-Marcel, C., Mucci, A., 2007. Oxygen isotope fractionation between synthetic aragonite and water: Influence of temperature and Mg2+ concentration. Geochim Cosmochim Ac 71, 4704-4715.

Kirkman, T.W. 1996. Statistics to use. Available at http://www.physics.csbsju.edu/stats/. (Last accessed September 8, 2018)

Klitgaard-Kristensen, D., Sejrup, H. -P., Haflidason, H., Johnsen, S., Spurk, M., 1998. A regional 8200 cal. yr BP cooling event in northwest Europe, induced by final stages of the Laurentide ice-sheet deglaciation? J Quaternary Sci 13, 165–169.

Kobashi, T., Severinghaus, J.P., Brook, E.J., Barnola, J.-M., Grachev, A.M., 2007. Precise timing and characterization of abrupt climate change 8200 years ago from air trapped in polar ice. Quat. Sci. Rev. 26, 1212–1222.

Kurita, N., Ichiyanagi, K., Matsumoto, J., Yamanaka, M.D., Ohata, T., 2009. The relationship between the isotopic content of precipitation and the precipitation amount in tropi- cal regions. J. Geochem. Explor. 102, 113–122.

Lachniet, M.S., 2009. Climatic and environmental controls on speleothem oxygen-isotope values. Quat. Sci. Rev. 28, 412–432.

Lambeck, K., Rouby, H., Purcell, A., Sun, Y., Sambridge, M., 2014. Sea level and global ice volumes from the Last Glacial Maximum to the Holocene. Proc. Natl. Acad. Sci. 111, 15296–15303.

LeGrande, A.N., Schmidt, G.A., 2008. Ensemble, water isotope-enabled, coupled general circulation modeling insights into the 8.2 ka event. Paleoceanography 23, PA3207. http://dx.doi.org/10.1029/2008PA001610.

LeGrande, A.N., Schmidt, G.A., Shindell, D.T., Field, C.V., Miller, R.L., Koch, D.M., Faluvegi, G., Hoffmann, G., 2006. Consistent simulations of multiple proxy responses to an abrupt climate change event. Proc. Natl. Acad. Sci. 103, 837–842.

Li, Y.-X., Renssen, H., Wiersma, A.P., Törnqvist,T.E., 2009. Investigating the impact of Lake Agassiz drainage routes on the 8.2 ka cold event with a climate model. Climate of the Past 5, 471–480.

Liu, Y. H., Henderson, G. M., Hu, C. Y., Mason, A. J., Charnley, N., Johnson, K. R., Xie, S. C., 2013. Links between the East Asian monsoon and North Atlantic climate during the 8,200 year event, Nat Geosci 6, 117–120, 10.1038/Ngeo1708.

Ljung, K., Bjorck, S., Renssen, H., Hammarlund, D., 2008. South Atlantic island record reveals a South Atlantic response to the 8.2 kyr event. Clim Past 4, 35–45.

Lunt, D.J., Dunkley Jones, T., Heinemann, M., Huber, M., LeGrande, A., Winguth, A., Loptson, C., Marotzke, J., Roberts, C.D., Tindall, J., Valdes, P., Winguth, C., 2012. A model–data comparison for a multi-model ensemble of early Eocene atmosphere–ocean simulations: EoMIP. Clim. Past 8, 1717-1736.

Lutjeharms, J.R.E., 2006. The Aghulas Current. Springer.

Lynch-Stieglitz, J., 2017. The Atlantic Meridional Overturning Circulation and Abrupt Climate Change. Annual Review of Marine Science 9, 83-104.

Marshall, J.D., Lang, B., Crowley, S.F., Weedon, G.P., van Calsteren, P., Fisher, E.H., Holme, R., Holmes, J.A., Jones, R.T., Bedford, A., Brooks, S.J., Bloemendal, J., Kiriakoulakis, K., Ball, J.D., 2007. Terrestrial impact of abrupt changes in the north Atlantic thermohaline circulation: early Holocene, UK. Geology 35, 639–642.

Massey, F.J., 1951. The Kolmogorov-Smirnov Test for Goodness of Fit. Journal of the American Statistical Association 46, 68–78.

Massé, G., Rowland, S.J., Sicre, M.A., Jacob, J., Jansen, E., Belt, S.T., 2008. Abrupt climate changes for Iceland during the last millennium: evidence from high resolution sea ice reconstructions. Earth and Planetary Science Letters 269, 565–569.

Matero, I.S.O., Gregoire, L.J., Ivanovic, R.F, Tindall, J.C., Haywood, A.M., 2017. The 8.2 ka cooling event caused by Laurentide ice saddle collapse. Earth and Planetary Science Letters 473, 205–214. https://doi.org/10.1016/j.epsl.2017.06.011.

McDermott, F., 2004. Palaeoclimate reconstruction from stable isotope variations in speleothems: a review. Quaternary Sci Rev 23, 901–918.

McDermott F., Schwarcz H. and Rowe P. (2006) Isotopes in speleothems. In Isotopes in Palaeoenvironmental Research (ed. M. Leng). Springer, Dordrecht, The Netherlands, pp. 185–226.

Mickler, P.J., Stern, L.A., Banner, J.L., 2006. Large kinetic isotope effects in modern speleothems. Geol Soc Am Bull 118, 65-81. doi:10.1130/B25698.1.

Meissner, K.J., Clark, P.U., 2006. Impact of floods versus routing events on the thermohaline circulation. Geophys. Res. Lett. 33, L15704. http://dx.doi.org/ 10.1029/2006GL026705.

Middleton, J., Middleton, V., 2002. Karst and caves of Madagascar. Cave Karst Sci. 29, 13–20.

Moore, G.W., 1956. Aragonite speleothem as indicators of paleotemperature. Am. J. Sci. 254, 746–753.

Morrill, C., Anderson, D.M., Bauer, B.A., Buckner, R., Gille, E.P., Gross, W.S., Hartman, M., Shah, A., 2013a. Proxy benchmarks for intercomparison of 8.2 ka simulations. Clim. Past 9, 423–432.

Morrill, C., LeGrande, A.N., Renssen, H., Bakker, P., Otto-Bliesner, B.L., 2013b. Model sensitivity to North Atlantic freshwater forcing at 8.2 ka. Clim Past 9, 955–968.

Morrill, C., Jacobsen, R.M., 2005. How widespread were climate anomalies 8200 years ago? Geophys. Res. Lett. 32, L19701. http://dx.doi.org/10.1029/ 2005GL023536.

Morse, J.W., Wang, Q., Tsio, M.Y., 1997. Influences of temperature and Mg/Ca ratio on $CaCO_3$ precipitates from seawater. Geology 25, 85–87.

Muller, J., Masse, G., Stein, R., Belt, S.T., 2009. Variability of sea-ice conditions in the Fram Strait over the past 30,000 years. Nature Geoscience 2, 772–776.

Murray, J.W., 1954. The deposition of calcite and aragonite in caves. J. Geol. 62, 481–492.

NASA Earth Observatory TRMM, 2016. Global Maps: Land Surface Temperature Anomaly. http://earthobservatory.nasa.gov/GlobalMaps/view.php?d1=MOD_LSTAD_M&d2 =TRMM_3B43M. Accessed August 26th, 2016.

Oster, J.L., Sharp, W.D., Covey, A.K., Gibson, J., Rogers, B., Mix, H., 2017. Climate response to the 8.2 ka event in coastal California. Sci Rep-Uk 7, 3886.

Paillard, D., Labeyrie, L., Yiou, P., 1996. Macintosh program performs time-series analysis, Eos Trans. AGU 77, 379.

Park, J., Park, J., Yi, S., Kim, J.C., Lee, E., Jin, Q., 2018. The 8.2 ka cooling event in coastal East Asia: High-resolution pollen evidence from southwestern Korea. Sci Rep-Uk 8, 12423.

Phipps, S.J., McGregor, H.V., Gergis, J., Gallant, A.J.E., Neukom, R., Stevenson, S., Ackerley, D., Brown, J.R., Fischer, M.J., van Ommen, T.D., 2013. Paleoclimate Data–Model Comparison and the Role of Climate Forcings over the Past 1500 Years. J Climate 26, 6915-6936.

Pobeguin, T., 1965. Sur les concretions calcaires observées dans la Grotte de Moulis (Ariège). CR Somm. Soc. Géol. Fr. 241, 1791–1793.

Pope, V.D., Gallani, M.L., Rowntree, P.R., Stratton, R.A., 2000. The impact of new physical parametrizations in the Hadley Centre climate model: Hadam3. Clim. Dyn. 160, 123–146.

Press, W.H., Teukolsky, S.A., Vetterling, W.T., Flannery, B.P., 1992. Numerical Recipes in C. 2nd edition. Cambridge University Press.

Railsback, L.B., Akers, P.D., Wang, L.X., Holdridge, G.A., Voarintsoa, N.R., 2013. Layer-bounding surfaces in stalagmites as keys to better paleoclimatological histories and chronologies. International Journal of Speleology 42, 167–180.

Railsback, L.B., Brook, G.A., Chen, J., Kalin, R., Fleisher, C.J., 1994. Environmental controls on the petrology of a Late Holocene speleothem from Botswana with annual layers of aragonite and calcite. J Sediment Res A 64, 147–155.

Rayner, D., Hirschi, J.J.M., Kanzow, T., Johns, W.E., Wright, P.G., Frajka-Williams, E., Bryden, H.L., Meinen, C.S., Baringer, M.O., Marotzke, J., Beal, L.M., Cunningham, S.A., 2011. Monitoring the Atlantic meridional overturning circulation. Deep-Sea Res Pt Ii 58, 1744-1753.

Renssen, H., Goosse, H., Fichefet, T., Campin, J.-M., 2001. The 8.2 kyr BP event simulated by a global atmosphere–sea-ice–ocean model. Geophys. Res. Lett. 28, 1567–1570.

Retrum, J. B., Gonzalez, L. A., Edwards, R., Cheng, H., Tincher, S. M., Urbani, F., 2013. A high-resolution stalagmite Holocene paleoclimate record from northern Venezuela with insights into the timing and duration of the 8.2 ka event. American Geophysical Union, Fall Meeting 2013, abstract #PP33C-1948

Rohling, E.J., Pälike, H., 2005. Centennial-scale climate cooling with a sudden cold event around 8,200 years ago. Nature 434, 975–979, doi: 10.1038/nature03421.

Romanek, C.S., Grossman, E.L., Morse, J.W., 1992. Carbon Isotopic Fractionation in Synthetic Aragonite and Calcite - Effects of Temperature and Precipitation Rate. Geochim Cosmochim Ac 56, 419-430.

Rozanski, K., Araguás-Araguás, L., Gonfiantini, R., 1993. Isotopic patterns in modern global precipitation. In: Swart, P.K., Lohmann, K.L., McKenzie, J., Savin, S. (Eds.), Climate Change in Continental Isotopic Records. Amer. Geophys. Union, 1–37.

Rubinson, M., Clayton, R.N., 1969. Carbon-13 fractionation between aragonite and calcite. Geochim Cosmochim Ac 33, 997-1002.

Rühs, S., Durgadoo, J.V., Behrens, E., Biastoch, A., 2013. Advective timescales and pathways of Agulhas leakage. Geophys Res Lett 40, 3997-4000.

Saint-Ours, J. D., 1959. Les phénomènes karstiques à Madagascar. Annales de Spéléologie 14, 275–291.

Saji, N.H., Goswami, B.N., Vinayachandran, P.N., Yamagata, T., 1999. A dipole mode in the tropical Indian Ocean. Nature 401, 360-363. Scholz, D., Hoffmann, D.L., 2011. StalAge - an algorithm designed for construction of speleothem age models. Quat. Geochronol. 6, 369–382.

Singarayer, J.S., Burrough, S.L., 2015. Interhemispheric dynamics of the African rainbelt during the late Quaternary. Quaternary Sci Rev 124, 48-67. Singarayer, J.S., Burrough, S.L., 2015. Interhemispheric dynamics of the African rainbelt during the late Quaternary. Quaternary Sci Rev 124, 48-67.

Sletten, H.R., Railsback, L.B., Liang, F.Y., Brook, G.A., Marais, E., Hardt, B.F., Cheng, H., Edwards, R.L., 2013. A petrographic and geochemical record of climate change over the last 4600 years from a northern Namibia stalagmite, with evidence of abruptly wetter climate at the beginning of southern Africa's Iron Age. Palaeogeogr Palaeocl 376, 149–162.

Stephens, M.A. 1970. Use of the Kolmogorov-Smirnov, Cramer-von Mises and related statistics without extensive tables. Journal of the Royal Statistical Society, Series B 32:115-122.

Stommel, H., 1958. The Abyssal Circulation. Deep-Sea Res 5, 80–82, Doi 10.1016/S0146-6291(58)80014- 4.

Street-Perrott, F. A., Perrott, R. A., 1990. Abrupt climate fluctuations in the tropics: The influence of Atlantic Ocean circulation. Nature 358, 607–612.

Tadross, T., Randriamarolaza, L., Rabefitia, Z., Yip, Z.K., 2008. Climate Change in Madagascar: Recent, Past, and Future. 18p. http://www.csag.uct.ac.za/~mtadross/Madagascar%20Climate%20Report.pdf

Tarutani, T., Clayton, R.N., Mayeda, T.K., 1969. The effect of polymorphism and magnesium substitution on oxygen isotope fractionation between calcium carbonate and water. Geochim Cosmochim Ac 33, 987-996.

Taylor, K. C., Mayewski, P. A., Twickler, M. S., Whitlow, S. I., 1996. Biomass burning recorded in the GISP2 ice core: A record from eastern Canada?: Holocene 6, 1–6.

Taylor, K.E., Stouffer, R.J., Meehl, G.A., 2012. An Overview of CMIP5 and the Experiment Design. B Am Meteorol Soc 93, 485-498.

Teller, J.T., Leverington, D.W., Mann, J.D., 2002. Freshwater outbursts to the oceans from glacial Lake Agassiz and their role in climate change during the last deglaciation. Quat. Sci. Rev. 21, 879–887.

Thomas, E.R., Wolff, E.W., Mulvaney, R., Steffensen, J.P., Johnsen, S.J., Arrowsmith, C., White, J.W.C., Vaughn, B., Popp, T., 2007. The 8.2ka event from Greenland ice cores. Quat. Sci. Rev. 26, 70–81.

Thornalley, D.J.R., Elderfield, H., McCave, I.N., 2009. Holocene oscillations in temperature and salinity of the surface subpolar North Atlantic. Nature 457, 711-714.

Thrailkill, J., 1971. Carbonate deposition in Carlsbad Caverns. J. Geol. 79, 683–695.

Tindall, J.C., Valdes, P.J., 2011. Modeling the 8.2 ka event using a coupled atmosphere-ocean GCM. Glob. Planet. Change 79, 312–321.

Tindall, J.C., Valdes, P.J., Sime, L.C., 2009. Stable water isotopes in HadCM3: isotopic signature of El Nin~o southern oscillation and the tropical amount effect. J. Geophys. Res. 114, D04111. http://dx.doi.org/10.1029/2008JD010825.

Törnqvist, T.E., Hijma, M.P., 2012. Links between early Holocene ice-sheet decay, sea- level rise and abrupt climate change. Nat. Geosci. 5, 601–606.

Valdes, P.J., Armstrong, E., Badger, M.P.S., Bradshaw, C.D., Bragg, F., Davies-Barnard, T., Day, J.J., Farnsworth, A., Hopcroft, P.O., Kennedy, A.T., Lord, N.S., Lunt D.J., Marzocchi, A., Parry L.M., Roberts W.H.G., Stone, E.J., Tourte, G.J.L., Williams, J.H.T., 2017. The BRIDGE HadCM3 family of climate models: HadCM3@Bristol v1.0. Geosci Model Dev Discuss 2017, 1–42.

Vare, L.L., Massé, G., Gregory, T.R., Smart, C.W., Belt, S.T., 2009. Sea ice variations in the central Canadian Arctic Archipelago during the Holocene. Quaternary Sci Rev 28, 1354–1366.

Vellinga, M., Wood, R. A., 2002. Global climatic impacts of a collapse of the Atlantic thermohaline circulation, Climatic Change, 54, 251–267, Doi 10.1023/A:1016168827653.

Vinther, B.M., Buchardt, S.L., Clausen, H.B., Dahl-Jensen, D., Johnsen, S.J., Fisher, D.A., Koerner, R.M., Raynaud, D., Lipenkov, V., Andersen, K.K., Blunier, T., Rasmussen, S.O., Steffensen, J.P., Svensson, A.M., 2009. Holocene thinning of the Greenland ice sheet. Nature 461, 385–388.

Voarintsoa, N.R.G., Brook, G.A., Liang, F.Y., Marais, E., Hardt, B., Cheng, H., Edwards, R.L., Railsback, L.B., 2017a. Stalagmite multi-proxy evidence of wet and dry intervals in northeastern Namibia: Linkage to latitudinal shifts of the Inter-Tropical Convergence Zone and changing solar activity from AD 1400 to 1950. Holocene 27, 384–396.

Voarintsoa, N.R.G., Wang, L., Bruce Railsback, L., Brook, G.A., Liang, F., Cheng, H., Lawrence Edwards, R., 2017b. Multiple proxy analyses of a U/Th-dated stalagmite to reconstruct paleoenvironmental changes in northwestern Madagascar between 370 CE and 1300 CE. Palaeogeography, Palaeoclimatology, Palaeoecology 469, 138–155.

Voarintsoa, N.R.G., Railsback, L.B., Brook, G.A., Wang, L., Kathayat, G., Cheng, H., Li, X., Edwards, R.L., Rakotondrazafy, A.F.M., Madison Razanatseheno, M.O., 2017. Three distinct Holocene intervals of stalagmite deposition and nondeposition revealed in NW Madagascar, and their paleoclimate implications. Clim. Past 13, 1771-1790.

von Cabanis, Y., Chabouis, L., Chabouis, F., 1969. Végétaux et Groupements végétaux de Madagascar I. Bureau pour le Dévelppement de la Production Agricole, Tananarive.

von Grafenstein, U., Erlenkeuser, H., Müller, J., Jouzel, J., Johnsen, S., 1998. The cold event 8200 years ago documented in oxygen isotope records of precipitation in Europe and Greenland. Clim. Dyn. 14, 73–81.

Vonmoos, M., Beer, J., Muscheler, R., 2006. Large variations in Holocene solar activity: constraints from ^{10}Be in the Greenland Ice Core Project ice core. Journal of Geophysical Research-Space Physics 111, A10105.

Wang, Y.J., Cheng, H., Edwards, R.L., He, Y.Q., Kong, X.G., An, Z.S., Wu, J.Y., Kelly, M.J., Dykoski, C.A., Li, X.D., 2005. The Holocene Asian Mon- soon: Links to solar changes and North Atlantic climate: Science 308, 854–857, doi: 10.1126/science.1106296

Wanner, H., Solomina, O., Grosjean, M., Ritz, S. P., and Jetel, M., 2011. Structure and origin of Holocene cold events, Quaternary Sci Rev, 30, 3109-3123, 10.1016/j.quascirev.2011.07.010.

Weaver, A. J., Bitz, C. M., Fanning, A. F., Holland, M. M., 1999. Thermohaline circulation: High-latitude phenomena and the difference between the Pacific and Atlantic. Annual Review of Earth and Planetary Sciences 27, 231–285, DOI 10.1146/annurev.earth.27.1.231.

Wiersma, A.P., Renssen, H., Goosse, H., Fichefet, T., 2006. Evaluation of different freshwater forcing scenarios for the 8.2 ka BP event in a coupled climate model. Clim. Dynam. 27, 831–849, doi:10.1007/s00382-006-0166-0.

Wiersma, A. P., Roche, D. M., Renssen, H., 2011. Fingerprinting the 8.2 ka event climate response in a coupled climate model, J Quaternary Sci 26, 118–127, 10.1002/jqs.1439.

Wiersma, A.P., Renssen, H., 2006. Model-data comparison for the 8.2 ka B.P. event: Confirmation of a forcing mechanism by catastrophic drainage of Laurentide Lakes. Quaternary Sci Rev 25, 63–88, doi: 10.1016/j.quascirev.2005.07.009.

Wiersma, A.P., 2008. Character and causes of the 8.2 ka climate event. Comparing coupled climate model results and palaeoclimate reconstructions, Department of Paleoclimatology and Geomorphology. Vrije Universiteit, Amsterdam, PhD Thesis. p. 160.

Wong, C.I., Breecker, D.O., 2015. Advancements in the use of speleothems as climate archives. Quaternary Sci Rev 127, 1–18.

World Bank Climate Change Knowledge Portal (CCKP) (2017). Historical Climate Data. Available from CCKP Website: http://sdwebx.worldbank.org/climateportal/index.cfm?page=downscaled_data_download&menu=historical. CCKP Metadata: http://sdwebx.worldbank.org/climateportal/doc/Metadata_2017.pdf. (Accessed, April 2018)

Wright, H.T., Vérin, P., Ramilisonina, Burney, D., Burney, L.P., Matsumoto, K., 1996. The evolution of settlement systems in the Bay of Boeny and the Mahavavy River Valley, northwestern Madagascar. Azania XXXI, 37–73.

Young, N.E., Briner, J.P., Rood, D.H., Finkel, R.C., 2012. Glacier Extent During the Younger Dryas and 8.2-ka Event on Baffin Island, Arctic Canada. Science 337, 1330.

Zhang, R., and Delworth, T. L., 2005. Simulated tropical response to a substantial weakening of the Atlantic thermohaline circulation, J Climate 18, 1853–1860, Doi 10.1175/Jcli3460.1,.

Zinke, J., Dullo, W.C., Heiss, G.A., Eisenhauer, A., 2004. ENSO and Indian Ocean subtropical dipole variability is recorded in a coral record off southwest Madagascar for the period 1659 to 1995. Earth Planet Sc Lett 228, 177-194.

Zoller, H., 1960. Pollenanalytische Untersuchungen zur Vegetationsgeschichte der insubrischen Schweiz. Denkschriften der Schweizerischen Naturforschenden Gesellschaft (in German). 83, 45–156. ISSN 0366-970X

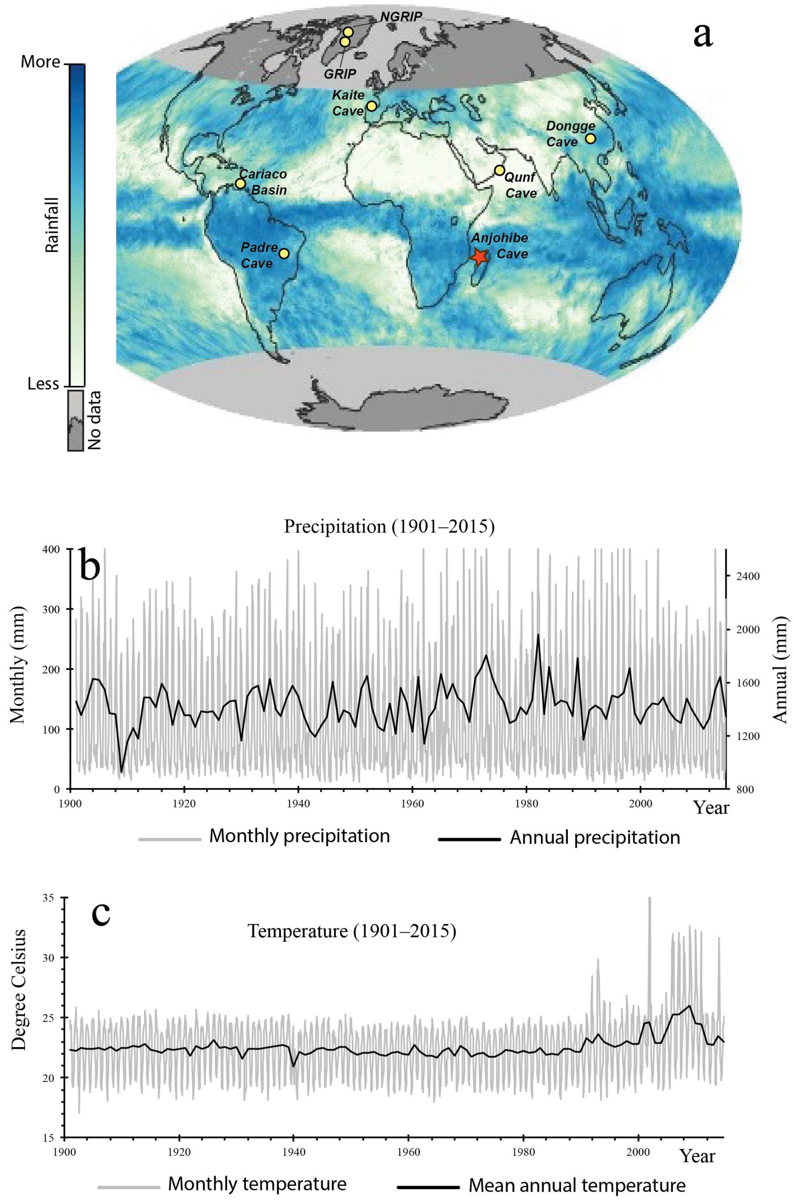

Figure 1: a) Global map from NASA Earth Observatory TRMM (2016) showing the geographic position of Madagascar and its position relative to the Inter-Tropical Convergence Zone (darker blue shading). The study location is indicated by a red star, and the other relevant locations discussed in the text are shown in yellow circle. b) Historical precipitation data from 1901 to 2015. c) Historical temperature data from 1901 to 2015. Historical climatology data (b–c) were produced

by the Climatic Research Unit (CRU) of University of East Anglia, and they made available at the World Bank Group Climate Change Knowledge Portal (2017).

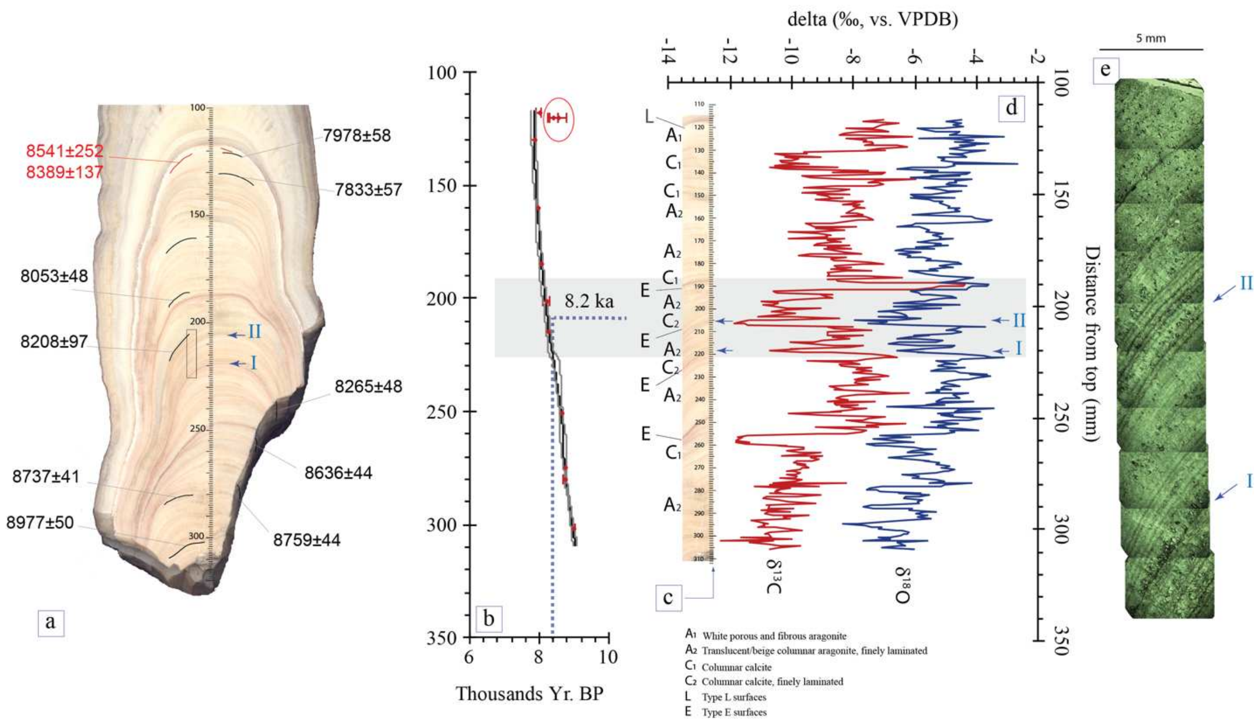

Figure 2: Stalagmite ANJB-2. a) Scanned image of the lower portion of Stalagmite ANJB-2 and the corresponding trenches for radiometric dating (black lines). The two blue arrows represent the first and second pulse, i.e. the onset of the 8.3 and 8.2 ka BP sub-events, respectively. Numbers in red are the rejected ^{230}Th data. Vertical rectangle is elaborated in Fig. 2e as a mosaic of photomicrographs. b) Age model built using StalAge of Scholz and Hoffman (2011; see Fig. S1 for details). Circled in red are the major outliers, rejected in the chronology reconstruction. c) Petrography and mineralogy logs using a slice from the stalagmite scan. d) Depth profile of $\delta^{18}O$ and $\delta^{13}C$. e) A mosaic of photomicrographs of selected section of the lower part of Stalagmite ANJB-2 (see Fig. 2a).

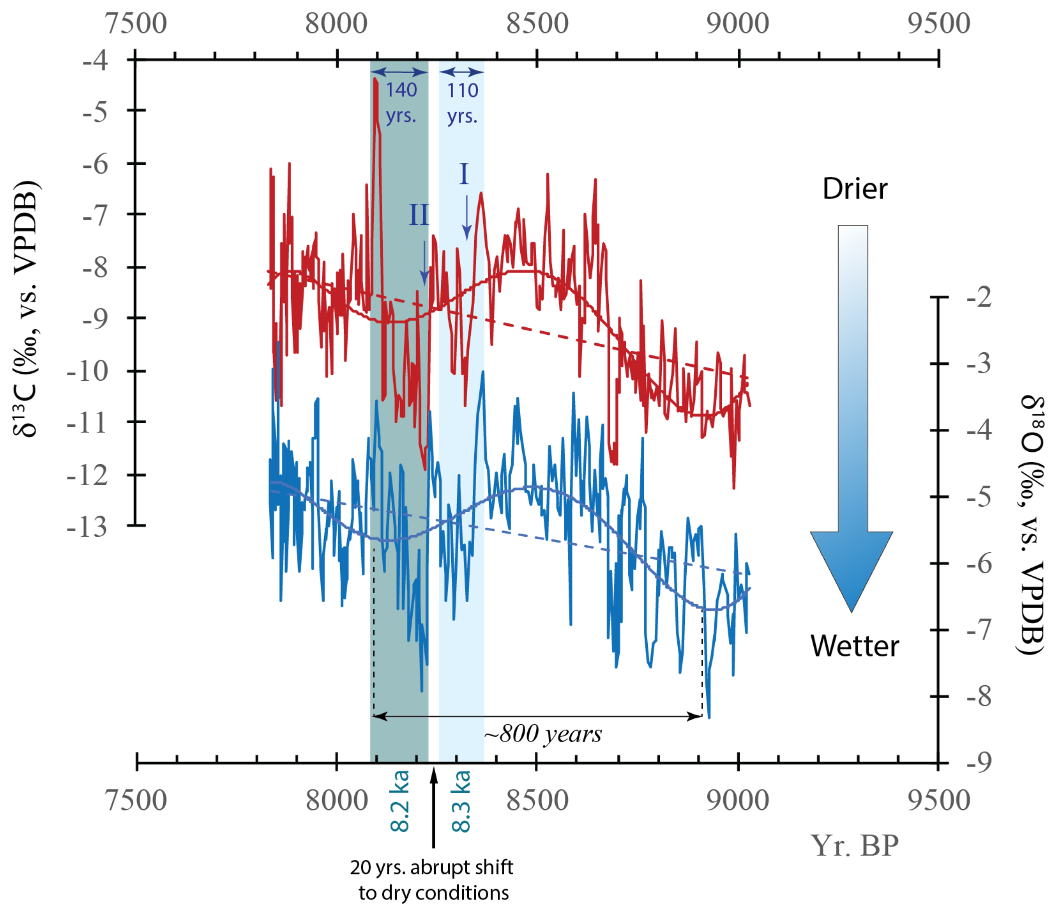

Figure 3: Timing and characteristics of the "8.2 ka" event in NW Madagascar. Blue thin vertical arrows represent the first and second pulse, i.e. the onset of the 8.3 and 8.2 ka BP event, respectively, similar to those in Fig. 2 (indicated with roman numbers I and II). Dashed blue and red lines represent the overall trend line of the isotopic records for $\delta^{18}O$ and $\delta^{13}C$, respectively. Smooth curves are polynomial curves fitting each isotopic point with a sine function.

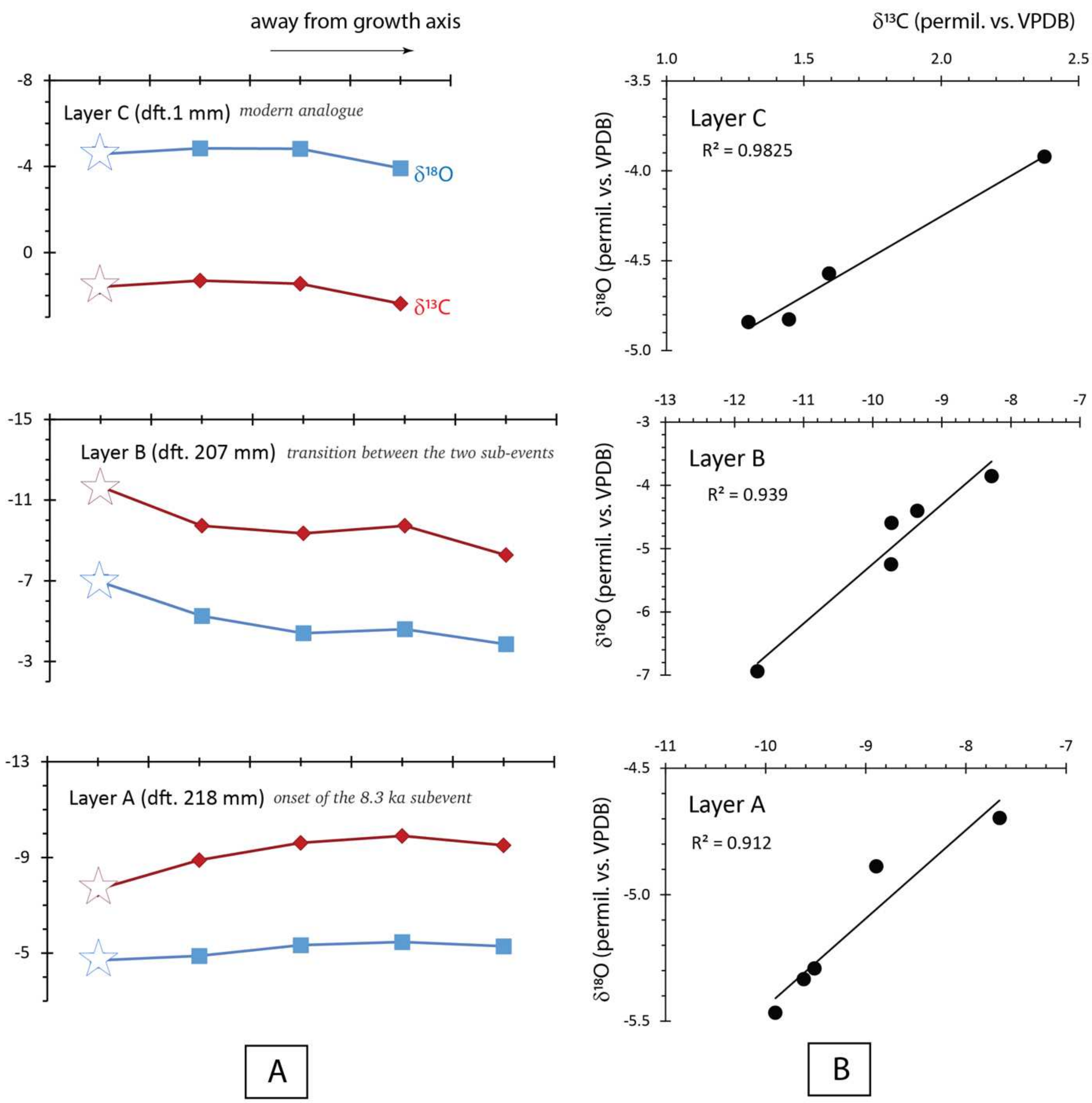

Figure 4: Layer-specific Hendy test on layers A, B, and C. The first $\delta^{18}O$ and $\delta^{13}C$ samples near the growth axis (indicated by stars) are old data, from 2015 measurement. New data points (2018) are in blue square and red diamonds. See text for discussion.

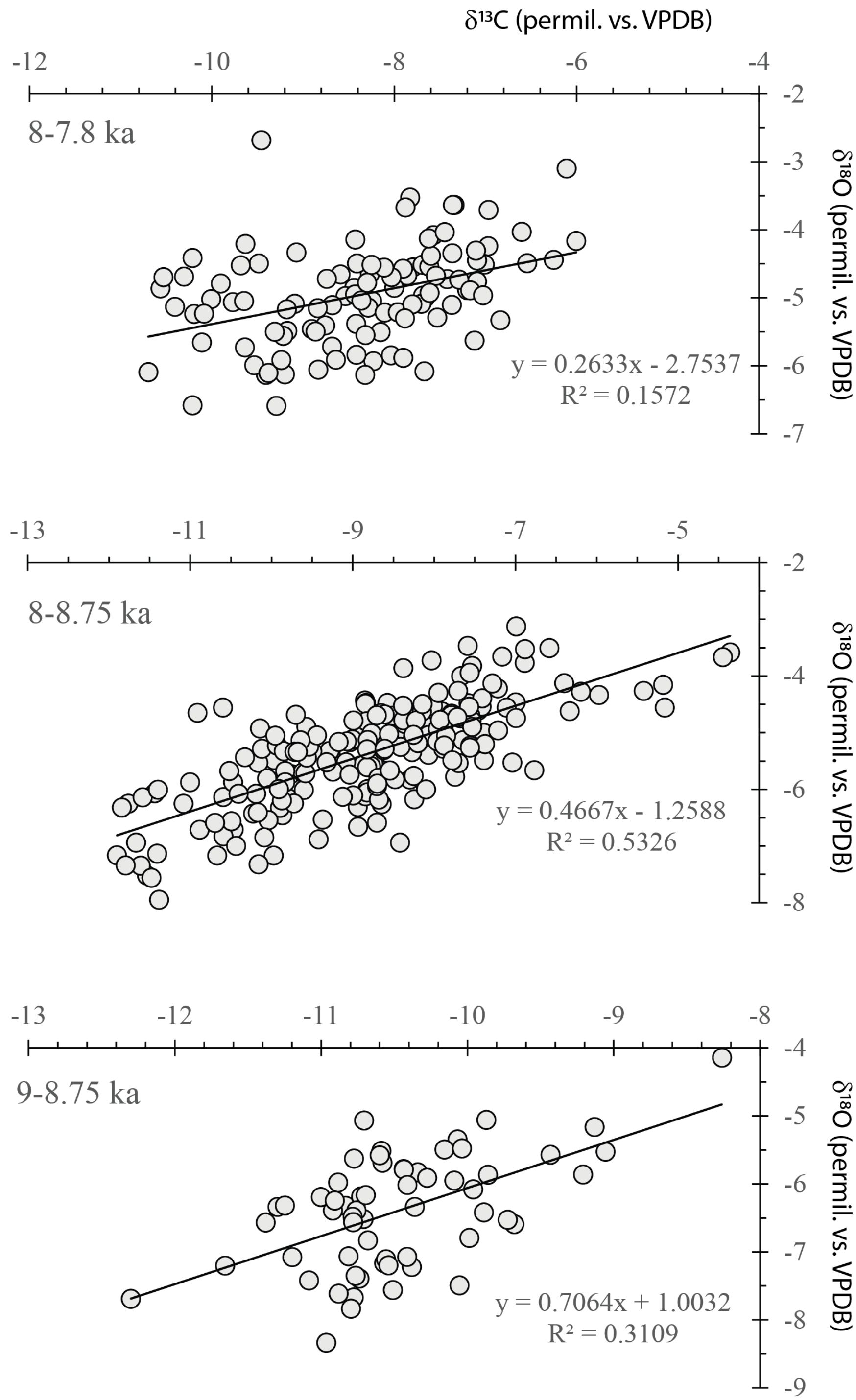

Figure 5: Hendy test along the growth axis of the lower 194 mm of Stalagmite ANJB-2, using the parametric Pearson correlation coefficient. The mathematical form of the correlation is expressed using the Major Axis of the Model II Regression.

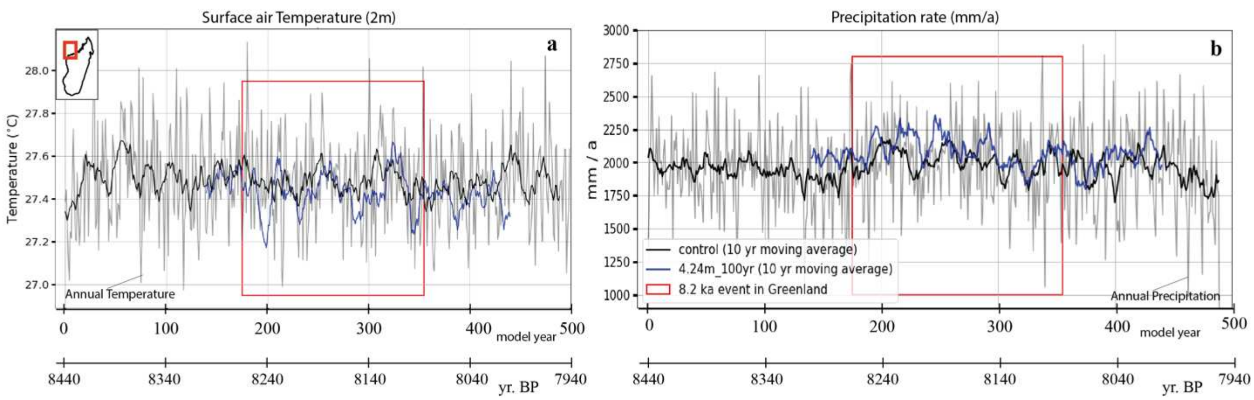

Figure 6: Time series for the modelled climate anomalies of the nearest grid box (centered at15°S, 45°E, shown in red square in the small inset figure) to Northwestern Madagascar for the saddle collapse simulation with respect to the control run with only the background freshwater flux of 0.05 Sv. a) Simulated surface air temperature (°C) time series. b) Simulated precipitation rate (mm/a) time series.

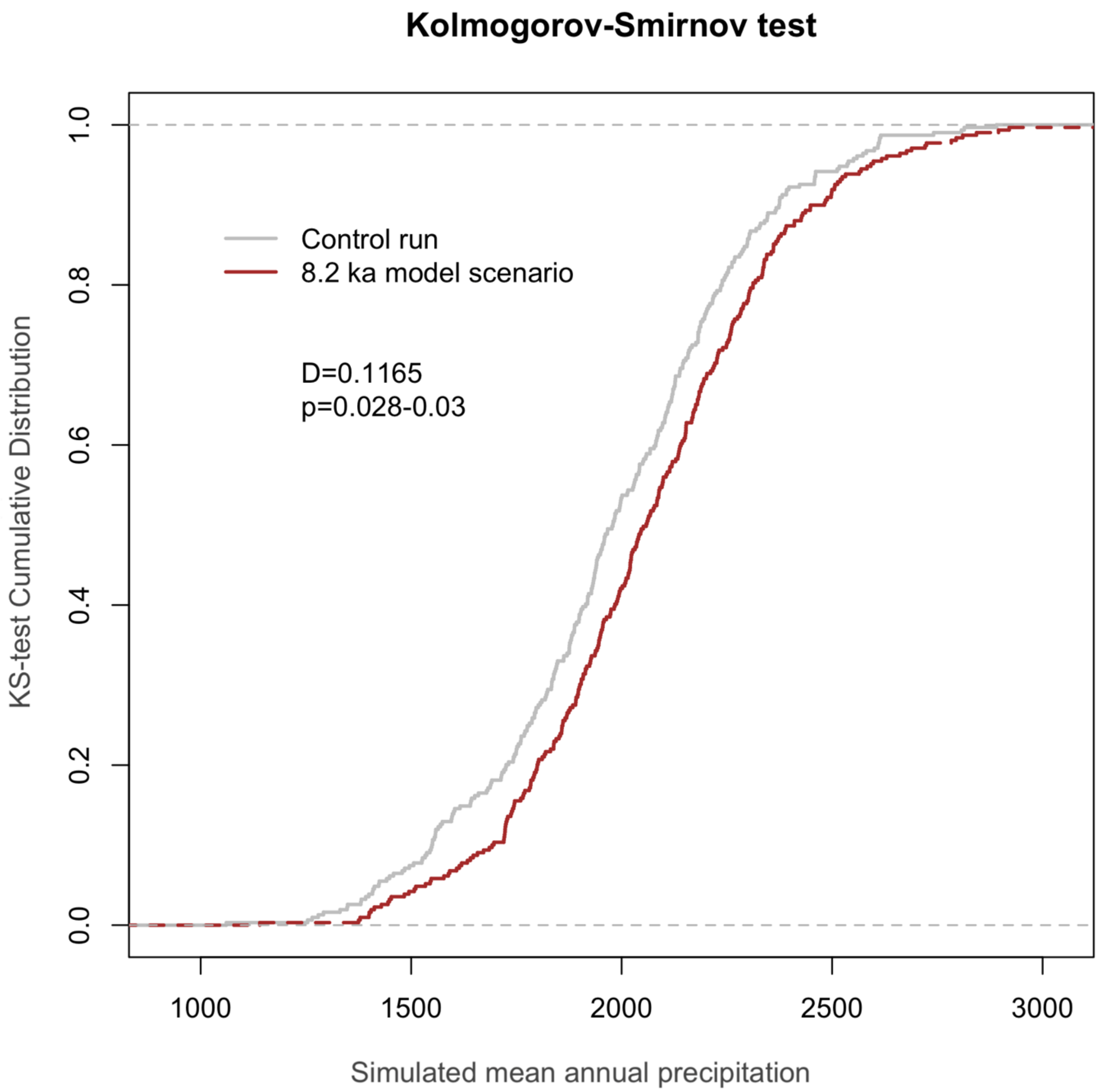

Figure 7: KS-test results between the control run and the 8.2 ka model scenarios in NW Madagascar.

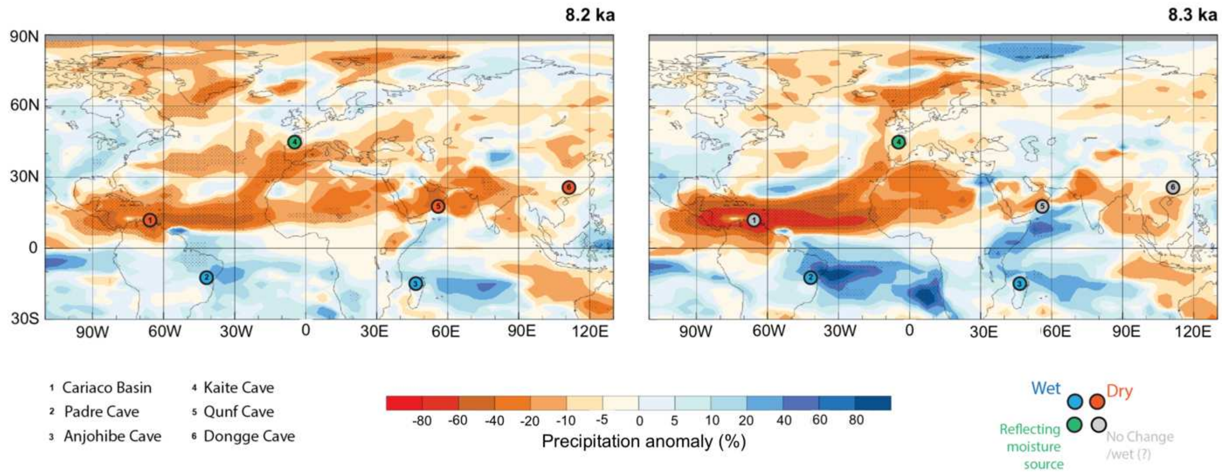

Figure 8: Maps of the modelled precipitation anomalies during the 8.3 ka and the 8.2 ka sub-events, with the six relevant locations and the climatic inferences from the paleoclimate proxies. The anomalies are calculated as annual means for a 30-yr period centered at the timing of the peak in the freshwater forcing. Stippling indicates significant difference at 99% level according to Welch's t-test.

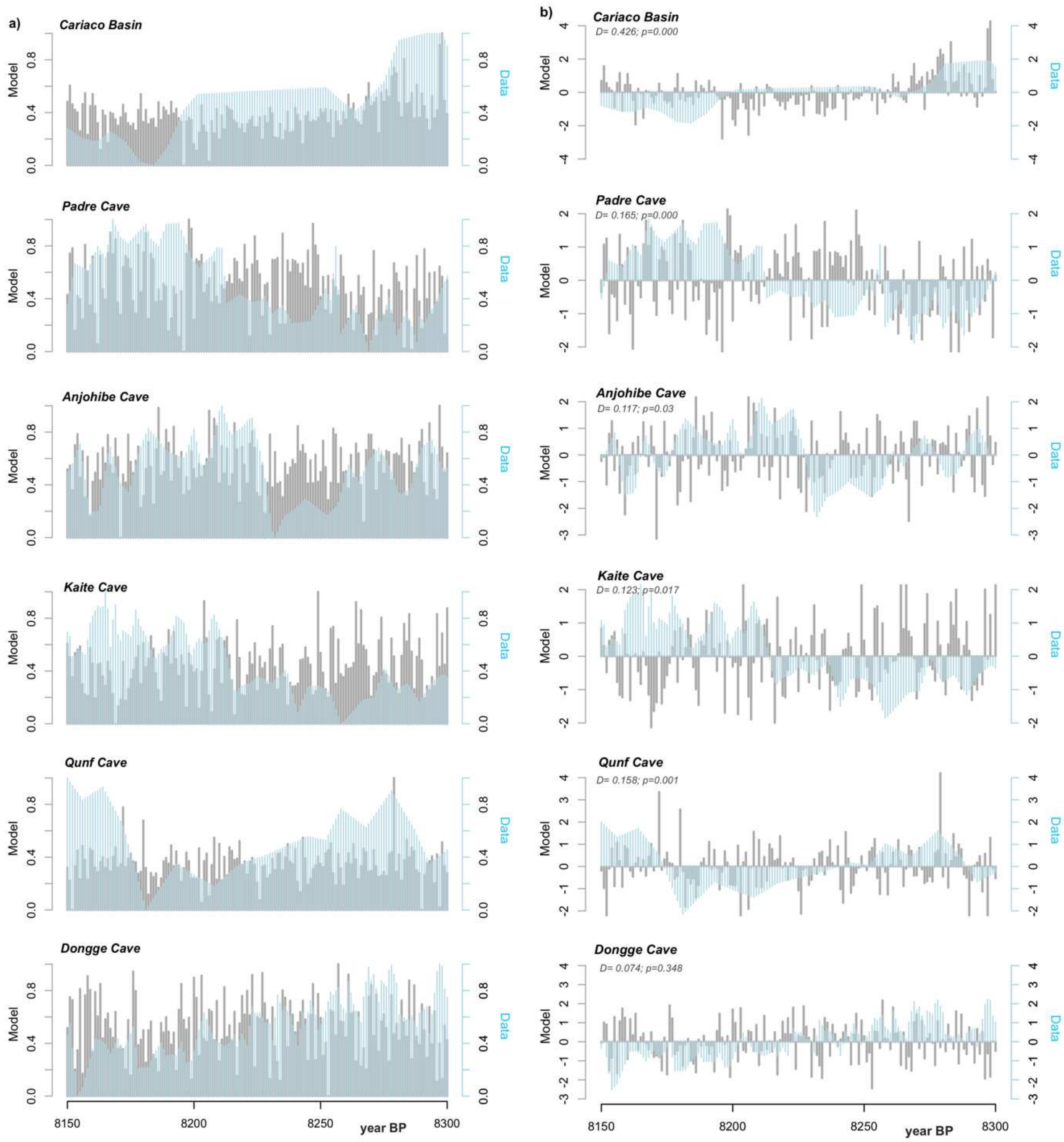

Figure 9: Data–model comparison for the six regions presented in Figs. 8 and 10B. a) Normalized values. b) Standardized values. D and p values in panel b represent the KS-test summary between model scenario and the control run for each location.

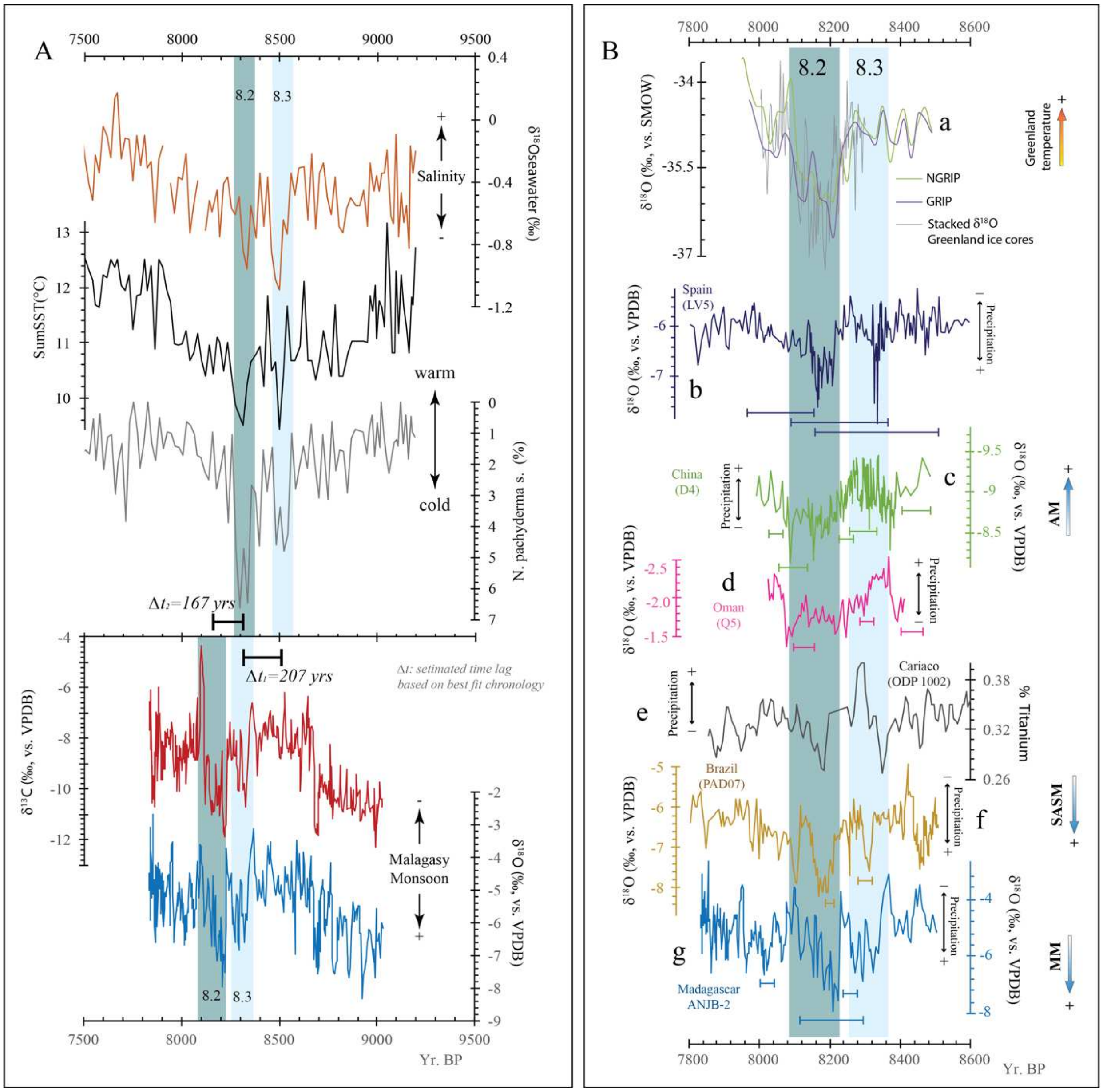

Figure 10: Global perspective of the 8.2 ka event. **A.** Comparison of the two wet phases (I, II) in Madagascar (this study) with the two cooling events (I, II) in the subpolar north Atlantic (top three profiles; Ellison et al., 2006). Δt_1 and Δt_2 are respectively the estimated time difference between the first/second cooling event and the first/second troughs in Stalagmite ANJB-2, using the best fit chronology of the samples' time series. See section 5.4.2 for discussion. **B.** The 8.2 ka in general perspective and corresponding monsoonal inferences from stalagmites isotopic records. a)

Greenland $\delta^{18}O$ from ice cores (Thomas et al., 2007; Vinther et al., 2009). b) Spain $\delta^{18}O$ from Stalagmite LV5 (Kaite Cave; Domínguez-Villar et al., 2009). c) China $\delta^{18}O$ from Stalagmite D4 (Dongge Cave; Cheng et al., 2009). d) Oman $\delta^{18}O$ from Stalagmite Q5 (Qunf Cave; Fleitmann et al., 2003). e) Venezuela sediment bulk titanium content (%) from ODP site 1002 (Cariaco Basin; Haug et al., 2001). f) Brazil $\delta^{18}O$ from Stalagmite PAD07 (Padre Cave; Cheng et al., 2009). g) Madagascar $\delta^{18}O$ from Stalagmite ANJB-2 (Anjohibe; this study). AM, SASM, and MM stand for Asian Monsoon, South American Summer Monsoon, and Malagasy Monsoon, respectively. Horizontal bars represent the age uncertainties for each corresponding record.

Table 1: ^{230}Th dates with 2 sigma error. ANJB-2-U120 and ANJB-2-U120R, bold italicized data, were rejected (see Fig. 2b).

Dft (mm)	Sample no.	^{238}U (ppb)		^{232}Th (ppt)		^{230}Th / ^{232}Th (atomic x10^{-6})		d^{234}U* (measured)		^{230}Th / ^{238}U (activity)		^{230}Th Age (yr) (uncorrected)		^{230}Th Age (yr) (corrected)		d^{234}U$_{Initial}$** (corrected)		^{230}Th Age (yr BP)*** (corrected)	
118	AB-2a	2569.8	±2.9	5266	±106	580.4	±11.9	7.5	±1.6	0.072126	±0.00032	8100	±40	8040	±58	7.6	±1.6	7978	±58
120	***ANJB-2-U120***	***1710***	***±4***	***20753***	***±418***	***108***	***±2***	***9.1***	***±2.3***	***0.0796***	***±0.0004***	***8955***	***±48***	***8605***	***±252***	***9***	***±2***	***8541***	***±252***
120	***ANJB-2-U120R***	***2075***	***±3***	***13340***	***±268***	***197***	***±4***	***6.3***	***±1.5***	***0.0767***	***±0.0003***	***8640***	***±38***	***8454***	***±137***	***6***	***±2***	***8389***	***±137***
130	ANJB-2-130	3042.4	±3.8	7448	±149	477	±10	6.2	±1.5	0.0709	±0.0002	7966	±26	7895	±57	6	±2	7833	±57
160	ANJB-2-160	2994.8	±4.1	2484	±50	1416	±29	4.3	±1.5	0.0712	±0.0002	8021	±30	7997	±35	4	±2	7935	±35
185	ANJB-2-U185	3490	±5	6040	±122	690	±14	3.6	±1.7	0.0724	±0.0003	8167	±33	8117	±48	4	±2	8053	±48
201	ANJB-2-U205	574	±1	1881	±38	374	±8	5.7	±1.8	0.0743	±0.0006	8367	±70	8272	±97	6	±2	8208	±97
215	ANJB-2-U215	3146	±4	5418	±109	713	±15	7	±1.5	0.0745	±0.0003	8379	±33	8329	±48	7	±2	8265	±48
251	ANJB-2-U251	4246	±5	7290	±147	745	±15	6.3	±1.3	0.0776	±0.0002	8750	±27	8700	±44	6	±1	8636	±44
275	ANJB-2-U275	6077	±9	9132	±184	861	±17	4.5	±1.5	0.0785	±0.0002	8867	±32	8823	±44	5	±2	8759	±44
280	ANJB-2-U280	5721	±18	5408	±110	1360	±28	2.4	±1.6	0.078	±0.0003	8828	±36	8801	±41	2	±2	8737	±41
302	ANJB-2-U302	9833	±44	1617	±33	8024	±166	5.2	±1.9	0.08	±0.0004	9045	±50	9041	±50	5	±2	8977	±50

U decay constants: $\lambda_{238} = 1.55125x10^{-10}$ (Jaffey et al., 1971) and $\lambda_{234} = 2.82206x10^{-6}$ (Cheng et al., 2013). Th decay constant: $\lambda_{230} = 9.1705x10^{-6}$ (Cheng et al., 2013).

*$\delta^{234}U = ([^{234}U/^{238}U]_{activity} - 1)x1000$. ** $\delta^{234}U_{initial}$ was calculated based on ^{230}Th age (T), i.e., $\delta^{234}U_{initial} = \delta^{234}U_{measured}\ x\ e\lambda^{234xT}$.

Corrected ^{230}Th ages assume the initial $^{230}Th/^{232}Th$ atomic ratio of $4.4 \pm 2.2\ x10^{-6}$. Those are the values for a material at secular equilibrium, with the bulk earth $^{232}Th/^{238}U$ value of 3.8. The errors are arbitrarily assumed to be 50%.

***BP stands for "Before Present" where the "Present" is defined as the year 1950 AD

Investigating the 8.2 ka event in northwestern Madagascar: insight from data–model comparisons

Ny Riavo G. Voarintsoa[1,*], Ilkka S.O. Matero[2], L. Bruce Railsback[1], Lauren Gregoire[2], Julia Tindall[2], Louise Sime[3], Hai Cheng[4,5], R. Lawrence Edwards[5], George A. Brook[6], Gayatri Kathayat[4], Xianglei Li[4], Amos Fety Michel Rakotondrazafy[7], and Marie Olga Madison Razanatseheno[7]

[1]*Department of Geology, University of Georgia, Athens, GA 30602-2501 U.S.A.*

[2]*University of Leeds, School of Earth and Environment, Leeds, LS2 9JT, UK*

[3]*Ice Dynamics and Paleoclimate, British Antarctic Survey, Cambridge CB3 0ET, UK*

[4]*Institute of Global Environmental Change, Xi'an Jiaotong University, Xi'an, Shaanxi 710049, P.R. China*

[5]*Department of Earth Sciences, University of Minnesota, Minneapolis, Minnesota 55455, U.S.A.*

[6]*Department of Geography, University of Georgia, Athens, Georgia, 30602-2502 U.S.A.*

[7]*Mention Sciences de la Terre et de l'Environnement, Domaine Sciences et Technologie, Université d'Antananarivo, Madagascar*

---

* Corresponding author:

E-mail address: nyriavony@gmail.com (Ny Riavo G. Voarintsoa)

Current address: *Institute of Earth Sciences, The Hebrew University in Jerusalem, Israel*

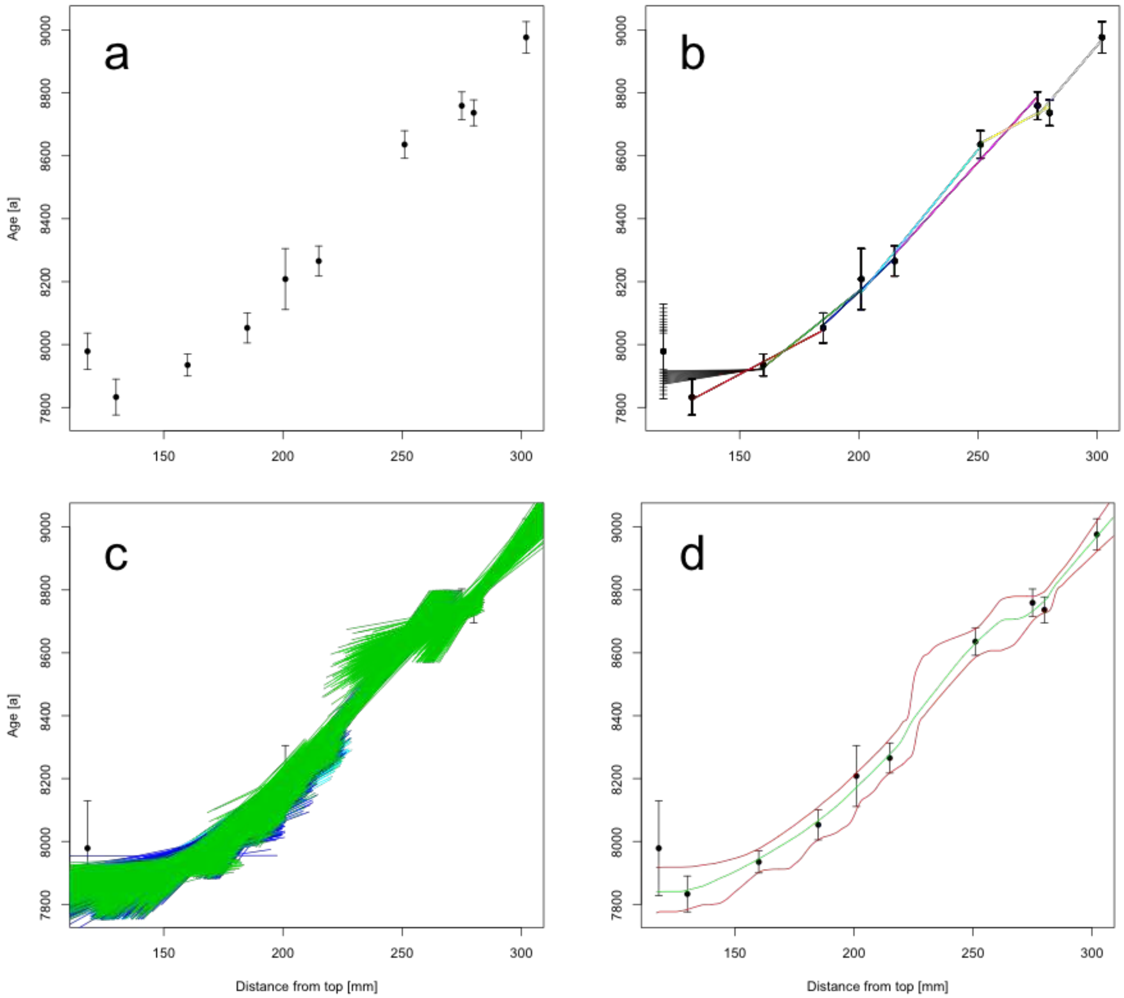

Figure S1: The four major steps in the StalAge chronology modelling for the basal age data of Stalagmite ANJB-2. a) Age data with corresponding original errors. b) identification of minor outliers. c) age modelling using the Monte Carlo simulation with different fits. d) final age model with the corresponding 95%-confidence limits.

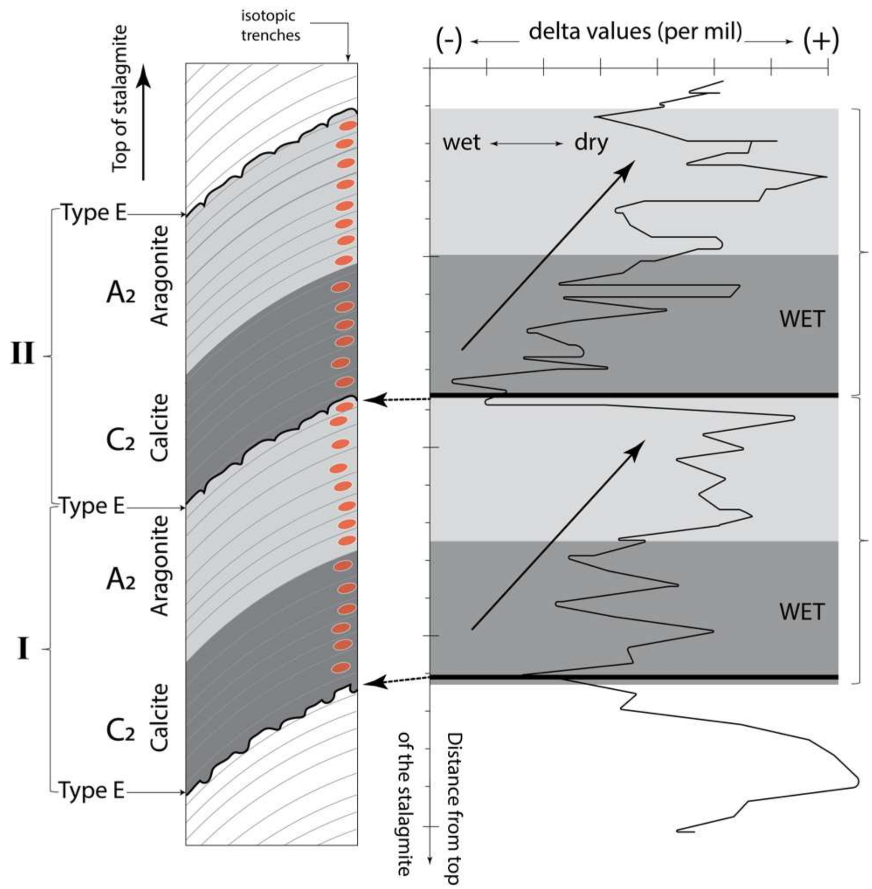

Figure S2: Simplified sketch showing the relationship between petrography, mineralogy, stable isotope fluctuation, and paleoclimate inferences. Roman numbers I and II are used here to represent the first and second sub-events, i.e. the 8.3 and 8.2 ka BP sub-event, respectively. Each sub-event starts with a Type E, i.e. erosional, surface and terminated with the deposition of aragonite. (see Sections 4.1 and 5.2).